Coral Reefs (2025) 44:1737–1757
https://doi.org/10.1007/s00338-025-02746-2

RESEARCH

A photophysiological model of coral bleaching simulates declines and recovery during an emulated multi-doldrum marine heatwave event

Sophia L. Ellis[1] · Mark E. Baird[2] · Peter Butcherine[1] · Amarah T. Fiori[3] · Luke P. Harrison[1] · Conor Hendrickson[1] · Kai G. Schulz[4] · Daniel P. Harrison[1,5]

Received: 5 February 2025 / Accepted: 29 August 2025 / Published online: 16 September 2025

Abstract Mass coral bleaching events have become increasingly frequent since the 1980s as sea surface temperatures have risen. Extremes of light and temperature stress leading to coral bleaching can develop when doldrum meteorological conditions occur during a marine heatwave event. The coral bleaching model simulates bleaching by tracking the build-up of reactive oxygen species driven by temperature-mediated, light-driven oxidative stress, triggering symbiont cell expulsion. This study is the first to evaluate the coral bleaching model for its ability to simulate heat and light stress dynamics in the coral *Acropora kenti* over multiple doldrum events *and* an intermediate recovery period. We tested model fidelity by comparing model predictions against laboratory measurements of coral bleaching stress taken during an emulated multi-doldrum marine heatwave event, incorporating artificial shade treatments. The model consistently predicted greater bleaching at increased temperatures and reduced shade levels, with an intermediate recovery period simulated between the doldrum events. Simulated bleaching stress captured up to fifty per cent of the variation in observed antioxidant enzyme activity. This study confirms that the significant emergent features of the model are present, as overall, the model adequately represented bleaching outcomes concerning the interactions between temperature and light. Thus, process-based modelling could be a valuable tool for predicting bleaching outcomes and optimising shading techniques, providing scientific managers with actionable strategies for mitigating coral bleaching.

Keywords Marine heatwave · Coral bleaching · Numerical model · Reactive oxygen species · Shading intervention

Introduction

The proportion of time the global ocean is subject to marine heatwave (MHW) conditions has increased by more than 50% from 1925 to 2016, relative to a fixed baseline (IPCC 2021; Oliver et al. 2018). MHWs, as defined by Hobday et al. (2016), are periods when sea temperatures exceed the 90th percentile of the local climatology for five days or more, regardless of season. Mass thermal coral bleaching events (CBEs) typically occur during summertime MHWs, and since 1998, the Great Barrier Reef (GBR) has experienced eight such events, with five occurring since 2016 (Cantin et al. 2024). The increasing occurrence and intensity of CBEs during these MHW conditions due to climate change have been of high concern since the 1990s (Hoegh-Guldberg 1999; Hughes et al. 2018). The frequency of MHWs is predicted to increase over the remainder of this

Supplementary Information The online version contains supplementary material available at https://doi.org/10.1007/s00338-025-02746-2.

✉ Sophia L. Ellis
sophia.ellis@scu.edu.au

1 School of Environment, Science and Engineering, National Marine Science Centre, Southern Cross University, Coffs Harbour, NSW 2450, Australia

2 Environment Research Unit, Commonwealth Scientific and Industrial Research Organisation, Hobart, TAS 7001, Australia

3 College of Science and Engineering, James Cook University, Townsville, QLD 4811, Australia

4 Centre for Coastal Biogeochemistry, School of Environment, Science and Engineering, Southern Cross University, Lismore, NSW 2480, Australia

5 School of Geosciences, University of Sydney, Sydney, NSW 2050, Australia

century (Oliver et al. 2019). Consequently, without intervention, mass bleaching events are likely to increase in both prevalence and severity (Hughes et al. 2018).

When elevated sea surface temperatures coincide with clear skies and transparent waters, light stress is intensified alongside heat stress during severe coral bleaching events (Baker et al. 2008; Mumby et al. 2001). Doldrums are equatorial regions of calm winds within the intertropical convergence zone and have been linked to mass CBEs (DeCarlo et al. 2017; Miller et al. 2009; Richards et al. 2024). During doldrum periods, reduced wind speeds lead to calmer surface conditions and increased settlement of particulate matter. These changes enhance the penetration of visible and ultraviolet light into the water column, as smoother surface conditions reflect less light and clearer water allows deeper transmission. Both factors can accelerate coral bleaching (Jones et al. 1998, 2000). The effects of temperature stress during a MHW on various coral genera have been investigated (Martell and Zimmerman 2021; Middlebrook et al. 2010; Sahin et al. 2023). However, model representations of coral response during simulated marine heatwaves with multi-doldrum periods are limited, underscoring the need for simulations that represent coral bleaching under the combined stressors of elevated irradiance and increased temperatures.

A recent meta-analysis concluded that reducing incident light with shade during heat stress could alleviate coral bleaching impacts (Tagliafico et al. 2022). Forms of natural shade observed in the reef environment include depth (Baird et al. 2018a), turbidity (Teixeira et al. 2019), shade from mangroves (Stewart et al. 2021), other coral colonies (Stimson 1985), self-shading within a colony (Anthony et al. 2005), and cloud presence (Leahy et al. 2013). Artificial shading was first experimented with using neutral-density screens (Coles and Jokiel 1978) and has since gained recognition as a viable strategy for preventing coral bleaching. Shading corals in aquaria can delay bleaching up to a moderate heat stress accumulation, preventing photochemical collapse (Ellis et al. 2024), and increasing the duration of shading can enhance protection against environmental stress factors (Butcherine et al. 2023). Shade cloth is a favoured option for reducing irradiance (Kramer et al. 2016; Tagliafico et al. 2022), though species-specific responses to shade cloth application (Butcherine et al. 2023; Ellis et al. 2024) and the scalability of this method present challenges for broader application (Harrison et al. 2019). To address these scalability constraints, fogging was proposed by the Reef Restoration and Adaptation Program as a regional-scale shading technique to reduce light stress at reef depth (Bay et al. 2019; Harrison 2024). Fogging is believed to be most applicable at low wind speeds, such as during doldrum periods. As reef interventions transition to deployment in natural reef environments, numerical modelling will be required to optimise deployment strategies. By extrapolating performance outcomes and quantifying potential risks, modelling will be crucial for evaluating shading as a scalable management tool for mitigating coral bleaching.

Numerical modelling is crucial in understanding symbiont photochemistry during coral bleaching events. The validation of coral physiological models ensures they accurately represent the sequence of events leading to bleaching (Ellis et al. 2025b) and remain a dynamic tool for management (Larsen et al. 2017). Model fidelity can be determined through evaluating how well model outputs align with photophysiological observations. Since different proxies capture distinct pathways in the bleaching cascade, selecting a representative proxy is critical to assessing model fit. Doing so will enhance predictive accuracy and deepen our understanding of the bleaching process.

Tracking the coral bleaching response can constrain the relative contributions of light and temperature to the bleaching process. The over-production of reactive oxygen species (ROS) and reduced repair or removal processes can lead to increased levels of oxidative damage under combined heat and light stress (Murphy et al. 2022). Proxies of oxidative stress in corals include members of the antioxidant system triggered by the in vivo generation of ROS, the photosystem efficiency of the coral's endosymbiotic algae, and visual indications of bleaching. However, the connections between bleaching cascades (e.g. photoinhibition) and endpoints (including mechanisms of symbiont loss, such as apoptosis, necrosis, and exocytosis) are poorly understood (Helgoe et al. 2024). Quantifying the individual pathways that lead to a photochemical, physiological, and visual response to environmental stress may inform the mechanisms of coral bleaching in a marine heatwave event and serve as benchmarks to validate physiological models predicting bleaching outcomes.

In this study, we examine whether a coral physiological model can accurately simulate a response to both an accumulation *and* recovery of heat and light stress over two distinct doldrum events in an emulated marine heatwave event. Bleaching simulated by the model was compared with observations of antioxidant enzyme activity, mean intensity of grey (MIG), and the number of fragment removals for *Acropora kenti*. We directly compared observed photosynthetic efficiency to the calculated model equivalent, and observed antioxidant enzyme activity was used to assess simulated bleaching stress. These results will determine whether mechanistic modelling from the perspective of the symbiont provides a realistic projection of coral bleaching outcomes over a theorised multi-doldrum marine heatwave-driven bleaching episode. By integrating experimental measurements with mechanistic modelling, this study contributes to an ongoing effort to predict the impacts of environmental stress on coral reef ecosystems.

Methods

Experimental incubations summary

Ten colonies of *Acropora kenti* (formerly *A. tenuis* (Bridge et al. 2023)) were collected from Davies Reef (18° 49.20S, 147° 38.82E), Great Barrier Reef (GBR), Australia, from a depth of between four and six metres. Previous experimentation using *A. kenti* has demonstrated that shade is ineffectual under heat stress (Ellis et al. 2024); however, there is a relevance to investigating the response of a model coral candidate such as *A. kenti*. *A. kenti* is an abundant coral species with a broad geographic distribution on the GBR and thus represents an ideal species to refine models of the coral–algae symbiosis (Messer et al. 2024). The subsampling of branches from *A. kenti* in the field provided intra-organism statistical replication.

The coral colonies were held at the National Sea Simulator facility, Australian Institute of Marine Science, Townsville, Australia, for three days before fragmentation. Each coral colony was fragmented into 150 × 5 cm fragments and then acclimated for 20 days under a maximum PAR of 150 µmol photons m^{-2} s^{-1} (daily light integral (DLI) of 4.13 mol photons m^{-2} d^{-1}). After acclimatisation, fifty *A. kenti* fragments from each of the ten genotypes were assigned between the experimental tanks (four replicate tanks per treatment equated to 36 × 50 L tanks). The experimental tanks were supplied with filtered (0.2 µm) flow-through seawater at 28.5°C (the maximum monthly mean (MMM) for the collection site) at 0.8 L min^{-1} and were circulated with a pump at ~ 1800 L h^{-1}.

A 70-day manipulative experiment tested the responses of *A. kenti* to an orthogonal combination of shade (three levels: an unshaded control, 15% and 30% shade) and temperature (three levels: ambient control, moderate heat stress, and high heat stress).

Windspeed data from the Bureau of Meteorology ACCESS-R model were extracted from the eReefs hydrodynamic model and used to estimate the wind conditions and identify doldrum occurrence. Doldrum duration and occurrence were determined using aggregated atmospheric, in-water, and modelled data from bleaching summers on the GBR, with a typical bleaching profile for individual reefs. The identified doldrum duration and occurrence pattern set the light and temperature regime. Water temperature data recorded at a depth of 4 m from the Davies Reef weather station in the Great Barrier Reef (1997–2022; AIMS 2020) were used to calculate the maximum monthly mean (MMM) of 28.5 °C, following the method described by Heron et al. (2016), with modifications to include only field-based measurements. Additionally, field data collected at 11 m depth during the summers of 2020 and 2021 were used to determine peak daily PAR and DLI experimental light intensity. A DLI of 15.95 mol photons m^{-2} d^{-1} (with a peak PAR of 585 µmol photons m^{-2} s^{-1}) was set to determine the normal summertime condition at 4 m on Davies Reef (N. Cantin & V. van Dongen-Vogels, personal communication, February 16, 2023). The proposed DLI for the 15% treatment was 13.75 mol photons m^{-2} d^{-1} (500 µmol photons m^{-2} s^{-1}); the proposed DLI for the 30% treatment was 11.28 mol photons m^{-2} d^{-1} (410 µmol photons m^{-2} s^{-1}). The light intensity was varied as a half-sine curve over a photoperiod with a 12 h light: dark cycle. The Degree Heating Weeks (DHW (°C-weeks)) were calculated for each temperature treatment.

The experiment consisted of two emulated 14-day doldrum events. The first doldrum event commenced one week after the start of the experiment. The time between the start of the experiment and the first doldrum event is referred to as the pre-doldrum event. Each doldrum event was split into a ramp-up period, the doldrum period itself, and a ramp-down period. Water temperatures were increased over 4–5 days in the ramp-up period of each doldrum event and decreased over 3–4 days in the ramp-down period at the end of each doldrum event to represent the slower increase and faster decrease in water temperature around doldrum periods. The time between the two doldrum events is the intermediate recovery period (days 30–35); the time between the second doldrum event and the end of the experiment is the recovery period post-doldrum two. The temperature of the intermediate recovery period and the recovery post-doldrum two was held below the MMM. The irradiance of the intermediate recovery period and the recovery post-doldrum two was lowered from values in the pre-doldrum period due to observations of progressed coral bleaching during the first doldrum event. Light intensity was decreased to a DLI of 8.25 mol photons m^{-2} d^{-1} with a maximum PAR (PAR_{max}) of 300 µmol photons m^{-2} s^{-1}.

Photosynthetically active radiation (PAR; µmol photons m^{-2} s^{-1}) was measured with Odyssey Submersible loggers (ODYPARW, Dataflow Systems Pty Ltd, New Zealand; 15 min interval; cross-calibrated against an LI-250A light meter with an attached LI-192 underwater quantum sensor (LI-COR®, USA)). One logger was placed in the experimental tank at coral depth for each light treatment. The PAR values were used to convert light panel intensity to the level of light received at the coral fragment depth. Temperature (°C) was averaged between values recorded by HOBO pendant loggers (HOBO MX2201, Onset, USA; 5 min interval, res: 0.04 °C) and by a series of DS18B20 temperature probes ($n = 7$) connected to the Seasim internal monitoring system.

To calculate dissolved inorganic nitrate and phosphate, 10 mL samples of incoming water were collected every four days ($n = 18$) and filtered through polyethersulfone hydrophilic, non-sterile 0.45 μm filters (Minisart®) into 10 mL polypropylene vials. Vials were immediately frozen (−18 °C) and stored for analysis. Concentrations of

ammonium (NH_4^+), nitrate (NO_3^-), and nitrite (NO_2^-) were determined using a SEAL Analytical AA3 Segmented Flow 5-Channel Analyser. Reagents produced a measurable colour change in the presence of the analytes, which were then measured by a colourimeter.

Coral fragments were fed once daily with green microalgae-enriched rotifers at a density of 0.35 individuals per millilitre of tank water per day (0.35 ind mL^{-1} d^{-1}) and non-enriched instar I *Artemia salina* at a density of 0.5 nauplii per millilitre of tank water per day (0.5 nauplii mL^{-1} d^{-1}). The incoming water flow rate was decreased during feeding. The concentration of particulate organic matter (POM) added to each 50 L tank at the time of feeding, with no water exchange, was calculated at 1019.25 mg m^{-3}, based on the combined dry weight of *Artemia salina* instar I nauplii (~2 µg) (Vanhaecke and Sorgeloos 1980) and rotifer nauplii (~0.3 µg) (Theilacker and Kimball 1984). The experimental tanks, including the pump, tank sides, and coral trays, were cleaned every two days or as necessary.

Experimental photochemical proxy

Coral photochemistry was measured by pulse amplitude modulated (PAM) fluorometry. Repeated measures were conducted every 4–6 days ($n = 13$). The fibre-optic probe of the PAM fluorometer (©Heinz Walz diving PAM I) was positioned ~ 3 mm away from the coral tissue. PAM settings: measuring light intensity = 8, measuring light frequency = 3, saturation width = 0.8, saturation intensity = 8, signal damping = 3, and gain = 2. Corals were low light adapted (~ 5 µmol photons m^{-2} s^{-1} for at least 20 min (Goyen et al. 2017)) before measurements of PSII photochemistry (F_v/F_m; dimensionless) were conducted ~ 1.5 h post-dawn.

Experimental visual proxy

The mean intensity of grey (MIG) is a colour analysis technique using digital photographs of coral fragments to quantify 'whiteness' (McLachlan and Grottoli 2021) and was used as a visual indication of coral health. Repeated measures of MIG were conducted every 4–6 days ($n = 14$). Algal overgrowth was removed before measurements. Images were taken of the coral fragments in their tanks from above at midday with consistent settings (Canon EOS R6 mirrorless, Canon RF 24–105 f/4–7.1 IS STM lens, SS: 1/60, focal length: 24 mm, manual white balance: 10000K, ISO-6400, F = 4) in a consistent light environment, with limited water distortion and surface reflection. A colour correction calibration card (Datacolour SpyderCheckr 24) was used to correct minute variations in lighting between images. Image corrections were performed in Adobe Lightroom Classic v12.2 and SpyderCheckr v1.6. In ImageJ (ver. 1.54d), a macro-function was used to outline the area of each coral fragment in the image. The average values of each RGB (red–green–blue) score were calculated and converted to 8-bit greyscale ((R + G + B)/3) to calculate the MIG for each fragment.

Experimental physiological proxies

This section details the methods used to determine the experimental proxies for evaluating model outputs.

Coral tissue extraction

Coral fragments were destructively sampled at 5, 19, 40, 54, and 68 days. Three fragments were randomly selected from each tank ($n = 108$ fragments taken per sampling event). Compressed air was used to extract coral tissue, and 2 mL of ice-cold 0.01 M phosphate-buffered saline (PBS) was added to each fragment to facilitate tissue removal. The removed tissue from each fragment and PBS mixture was collected in plastic bags and split equally between two 2 mL pre-weighed tubes (Rangel et al. 2019). Tubes were shaken, snap-frozen in liquid nitrogen, and stored at − 80 °C until analysis.

Biochemical assays

From one tissue sample (Tube 1), the total soluble protein content and catalase (CAT) activity were determined. From the second tissue sample (Tube 2), the total superoxide dismutase (SOD) activity and total soluble protein content were determined. SOD- and CAT-specific activity was normalised to protein content (units (U) mg^{-1} protein). All analyses used a BioTek Synergy H4 Microplate Reader and were corrected for path length. To determine tissue wet weight, tubes 1 and 2 for each coral fragment were centrifuged at 3500 × *g* for 5 min at 4 °C. The supernatant was discarded, and the resultant tissue was weighed.

Tube 1 samples were transferred into a 10 mL polypropylene tube containing 2 mL of PBS (3 mL final volume). The pellet from Tube 2 samples was resuspended in ice-cold PBS at 80 mg tissue mL^{-1}, vortexed, and then transferred into a 10 mL polypropylene tube. Tubes 1 and 2 samples were pulsed (~ 15 s) with a stick homogeniser (IKA ULTRA-TURRAX T 10; 10,000 rpm).

To determine protein concentration from Tubes 1 and 2, 200 µL of the homogenate was transferred into an empty microcentrifuge tube on ice containing 1 mL of PBS and then centrifuged at 7000 × *g* for 5 min at 4 °C. Protein in the cell lysate was determined at 595 nm following Bradford (1976), with bovine serum albumen as the standard. Protein concentration was estimated from a standard curve and expressed as mg mL^{-1}. A 150 µL or 5 µL aliquot of tissue homogenate was used to analyse for a low- or high-protein concentration, respectively (Bradford 1976).

For the analysis of CAT, a 50 µL aliquot of tissue homogenate from Tube 1 was used to estimate CAT activity at 240 nm every 30 s for 4 min following Beers and Sizer (1952), with modifications for the microplate (Li and Schellhorn 2007). The change in absorbance of 0.01 M hydrogen peroxide (H_2O_2) was used to estimate CAT activity using a molar extinction coefficient of 43.6 M^{-1} cm^{-1}. The CAT-specific activity was expressed as U mg^{-1} protein, in which 1 unit of CAT is required to decompose 1.0 µM of H_2O_2 per minute at 25 °C (Weydert and Cullen 2010).

For the analysis of SOD, a 200 µL aliquot of the tissue homogenate from Tube 2 was used to measure the inhibition of nitroblue tetrazolium reduction with xanthine-xanthine oxidase as a superoxide generator (Sun et al. 1988). The reaction mix was incubated at 25 °C for 30 min, and the absorbance change at 560 nm was compared to a standard curve to estimate percentage inhibition. The total SOD-specific activity was expressed as U mg^{-1} protein.

Fragment removals

During the experiment, compromised fragments (> 70% tissue removal – visual inspection) were removed from each experimental tank to preserve the remaining coral fragments. The total number of removals per treatment per day was recorded.

Statistical analysis

Independent replicates were used to test for significant differences ($\alpha \leq 0.05$) in CAT and SOD activity at five destructive sampling points (0, 19, 40, 54, and 68 days). A permutational multivariate analysis of variances (PERMANOVA) was conducted using Primer v6 & PERMANOVA + (Clarke and Gorley 2006), following the framework of Anderson (2017). The model included the factors shade (fixed, 3 levels), temperature (fixed, 3 levels), and tank (random, 36 levels), nested within temperature × shade.

From the above factorial structure, shade and temperature were used to test for differences in the number of removals per tank. To test the repeated measures F_v/F_m (13 time points) and MIG (14 time points) data, time was added as a fixed factor (13 or 14 levels) to the above factorial structure. Where significant variation was observed among tanks nested within temperature x shade, a permutational analysis of multivariate dispersion (PERMDISP) was performed to determine whether the significance was due to differences in dispersion rather than location. No significant differences in dispersion were detected for SOD and CAT, indicating that the observed tank effect was not driven by heterogeneity of variances; the significant tank effect was not investigated further. Genotype was excluded from the final model as no significant differences were observed between genotype levels. All statistical tests used pair-wise comparisons when significant main effects or their interactions were detected. PERMANOVA analyses were based on a normalised Euclidean distance dissimilarity matrix, used Type III sum of squares, and were run with 9999 iterations using permutation of residuals under a reduced model.

Linear regression analysis tested for a statistically significant relationship ($\alpha \leq 0.05$) between the activity of the antioxidant enzymes CAT and SOD, between CAT activity and simulated ROS concentration, and between SOD activity and simulated ROS concentration. CAT or SOD activity values collected for the same treatment at the same time point were averaged. Regression analyses were conducted in MATLAB (2023).

Model description

The coral bleaching model (CBM) has been applied in multi-year simulations within the CSIRO eReefs Environmental Modelling Suite (Baird et al. 2021, 2018b) and is a valuable tool for assessing management strategies on the GBR (Scofield et al. 2024). Model parameters were derived from a laboratory study using cultures of *Symbiodinium* phylotypes (Suggett et al. 2008). A one-polyp configuration of the CBM was developed to facilitate model assessment against laboratory experiments (Ellis et al. 2025b).

The CBM uses a process-based representation of the coral–symbiont relationship. The simulated expulsion of symbiont cells from the host is the bleaching mechanism resulting from temperature-mediated, light-driven oxidative stress. The expulsion rate depends on the temperature-mediated build-up of ROS concentration surpassing a ROS threshold of 1.42×10^{-14} mg O $cell^{-1}$ under excess light. Below the ROS threshold, no bleaching occurs (Suggett et al. 2009). ROS concentration and symbiont cell expulsion rate are hereafter termed ‘simulated bleaching stress’ and ‘simulated bleaching’, respectively.

To mechanistically represent ROS-driven bleaching, the model explicitly represents coral host biomass, symbiont biomass, intracellular pigment concentration, and nutrient status. The model’s photophysiological processes, including photoadaptation, xanthophyll cycle dynamics, and reaction centre state transitions, are quantified into model outputs. For a full explanation of model formulations, see Baird et al. (2018b) and Baird et al. (2021). The core elements of the model are also explained in Ellis et al. (2025b). A summary of the model is given below.

The symbiont model photosystem is divided into pigment and reaction centre dynamics, where absorbed photons influence carbon reserves, reaction centre state, or ROS concentration. Photochemical quenching occurs when chlorophyll *a* and photosynthetic pigments (xanthophyll diadinoxanthin) absorb photons, and electrons are passed to reaction centres;

non-photochemical quenching dissipates excess photon energy as heat via photoprotective pigments (xanthophyll diatoxanthin). The model represents the xanthophyll cycle as the switching between photosynthetic and photoprotective pigments, depending on the fraction of active to inactive reaction centres.

Symbiont growth depends on internal nitrogen, phosphorus, and carbon reserves, which are shared across the symbiont cell population and consumed to form structural material at the Redfield ratio. Photon absorption drives the process from carbon to fixed carbon; fixed carbon is assimilated for symbiont cell growth. The internal reserves of nitrogen, phosphorus, and carbon increase when the nutrient supply exceeds the consumption for growth, and decrease when the consumption for growth exceeds the nutrient supply (Baird et al. 2003). Diffusion-limited nutrient uptake increases reserve levels. Pigment synthesis adjusts based on photosynthetic efficiency, self-shading, and the fraction of inhibited reaction centres (Baird et al. 2018b).

Carbon fixation is mediated by the ribulose-1,5-bisphosphate carboxylase/oxygenase (RuBisCO) enzyme, with its activity controlled by a temperature-dependent formulation, where a positive temperature anomaly reduces the rate of carbon fixation. The NOAA bleaching index threshold links a 1 °C anomaly above climatological MMM to reduced RuBisCO activity (Baird et al. 2018b). Reaction centres transition between oxidised, reduced, and inhibited states, influencing ROS generation. The repair of inhibited reaction centres to an oxidised state is temperature-dependent, with the rate set to be able to repair damage inflicted by 10 mol photons m^{-2} d^{-1} light. Photon absorption rates dictate reaction centre transitions and ROS production, with a stoichiometric ratio of the number of photons that generate ROS set at 7000 mol photons (mg O_2)$^{-1}$.

In the model state variables, carbon, phosphorus, and nitrogen reserves were quantified as the concentration per unit area of the symbiont cell population (hereafter referred to as symbiont carbon, phosphorus, and nitrogen reserves). Symbiont nutrient fluxes include nutrient uptake from the overlying water column. We also present internal carbon, phosphorus, and nitrogen reserves as a normalised value, normalised to the maximum of that reserve that can be stored within the population (hereafter referred to as internal carbon, phosphorus, and nitrogen reserves), resulting in a value between 0 and 1. The chlorophyll *a*, photosynthetic, and photoprotective pigments were quantified as the concentration per unit area of the symbiont cell population. The reaction centre states of oxidised, reduced, and inhibited were presented as a normalised value, normalised to the total number of reaction centres.

Model configuration

The single-polyp version of the CBM configured in Ellis et al. (2025b) provided an enhanced representation of coral responses. The model originally allowed detoxification to reduce ROS to zero (Baird et al. 2018b). Revisions presented in Ellis et al. (2025b) included reducing the number of photons that lead to the generation of one ROS, altering the equation for ROS detoxification and removing the ROS loss coefficient. This configuration of the CBM was used to simulate coral responses here.

The environmental data of irradiance, temperature, and nutrients recorded in the experiment (outlined above) were used as forcings in the CBM. A single-value input forcing for particulate organic matter concentration was provided for each simulation (outlined above; 1019.25 mg m^{-3} d^{-1}). The MMM was input as 28.5 °C. A four-day spin-up period of ambient environmental data gave initial values for oxidised, reduced, and inhibited reaction centre concentration. The revised model configuration (Ellis et al. 2025b; Table 1) provided the initial conditions for symbiont biomass, chlorophyll *a* concentration, and ROS concentration. For a list of initial conditions of state variables used in the configuration to run the model, see

Table 1 Initial conditions of state variables used in model configuration

Symbol	Description	Value	Units
CS	Symbiont biomass	1	mg N m^{-2}
R_N	Reserves of nitrogen	CS*0.5	mg N m^{-2}
R_P	Reserves of phosphorus	CS*(1*((1/16)*(30.97/14.01)))*0.5	mg P m^{-2}
R_C	Reserves of carbon	CS*((106/16)*(12.01/14.01))*0.5	mg C m^{-2}
Chl	Symbiont chlorophyll *a* concentration	CS*5.6786/30	mg m^{-2}
X_p	Symbiont diadinoxanthin concentration	Chl*0.2448*0.33	mg m^{-2}
X_h	Symbiont diatoxanthin concentration	Chl*0.2448*0.67	mg m^{-2}
Q_{ox}	Oxidised reaction centre concentration	8.3213×10^{-11}	mg m^{-2}
Q_{red}	Reduced reaction centre concentration	7.7056×10^{-11}	mg m^{-2}
Q_{in}	Inhibited reaction centre concentration	4.2112×10^{-8}	mg m^{-2}
[ROS]	Reactive oxygen species concentration	ROSthreshold * 0.5	mg O cell^{-1}

ROSthreshold = 1.42×10^{-14} mg O cell^{-1}

Table 1. The simulation timeframe was 70 days. Model simulations were run in MATLAB (2023). See Data Availability for access to the model code.

Model validation

The CBM was validated using photochemical, visual, and physiological proxies of coral health recorded in the experiment. Observations of catalase and superoxide dismutase antioxidant activity, the mean intensity of grey, and the cumulative number of removals (outlined above) were compared to bleaching stress and bleaching simulated by the model. Observed PSII photochemistry (F_v/F_m) was compared to the model equivalent—the oxidised fraction of reaction centres (Eq. (1)). This represents the quantum efficiency of photosystem II if all functioning reaction centres are open:

$$\left(F_v/F_m\right)_{model} = \left(Q_{ox}/Q_T\right) \quad (1)$$

where Q_{ox} is the concentration of oxidised reaction centres, and Q_T is the total reaction centre concentration (Eq. (2)):

$$Q_T = Q_{ox} + Q_{red} + Q_{in} \quad (2)$$

where Q_{red} is the concentration of reduced reaction centres, and Q_{in} is the concentration of inhibited reaction centres. Model F_v/F_m was calculated for the same time F_v/F_m was measured in the experiment.

Results

Environmental data

The ambient temperature treatment (28.3 ± 0.2 °C (average ± SD)) remained below the MMM and thus accumulated no heat stress (Fig. 1a). The moderate heat stress treatment accumulated a total of 3 °C-weeks, separated into 1.7 °C-weeks during the first doldrum event and 1.3 °C-weeks during the second (Fig. 1b) During these events, the temperature was 30.75 ± 0.15 °C in the first doldrum period and 30.64 ± 0.15 °C in the second. The high heat stress temperature treatment accumulated a total of 4.6 °C-weeks, separated into 2.6 °C-weeks during the first doldrum event and 2 °C-weeks during the second (Fig. 1c). During these events, the temperature was 31.39 ± 0.17 °C in the first doldrum period and 31.19 ± 0.17 °C in the second. The first and second doldrum events lasted 16 and 14 days, respectively, for all treatments. In the pre-doldrum period (days 0–4), peak irradiance was recorded at 188.37 µmol photons m^{-2} s^{-1} (DLI 5.55 mol photons m^{-2} d^{-1}) (Fig. 1d). In the intermediate recovery period (days 30–35), peak irradiance was reduced to 108.03 µmol photons m^{-2} s^{-1} (DLI 3.32 mol photons m^{-2} d^{-1}). During the doldrum periods, the irradiance peaked at 344.46 µmol photons m^{-2} s^{-1} (DLI 10.23 mol photons m^{-2} d^{-1}), 292.79 µmol photons m^{-2} s^{-1} (DLI of 8.69 mol photons m^{-2} d^{-1}), and 241.12 µmol

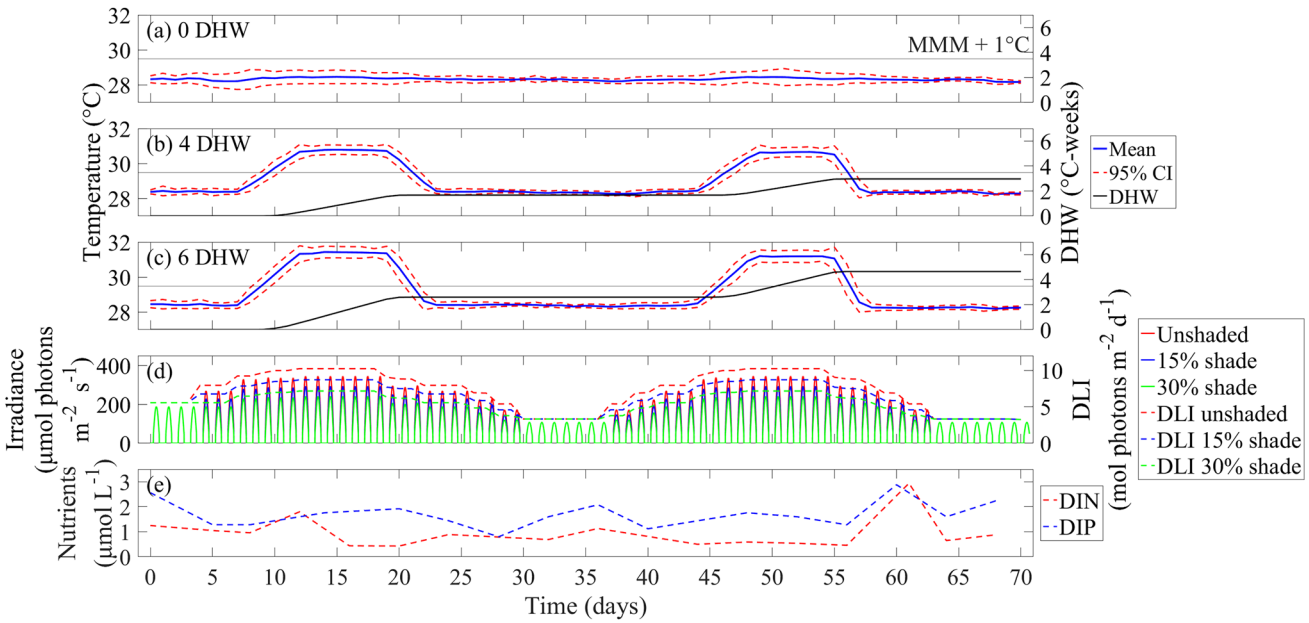

Fig. 1 Recorded water temperature (mean temperature (°C) of the day with 95% confidence limits (CL)) and Degree Heating Weeks (DHW (°C-weeks)) accumulation for the ambient temperature (nominal 28.4 °C) (**a**), moderate heat stress (**b**) and high heat stress (**c**) treatments, and maximum monthly mean (MMM; 28.5 °C) + 1 °C. PAR irradiance (µmol photons m^{-2} s^{-1}) and daily light integral (DLI; mol photons m^{-2} d^{-1}) at the depth of coral fragments, in the unshaded, 15% and 30% shade treatment (**d**). The concentration of dissolved inorganic nitrogen (DIN; µmol L^{-1}) and phosphorus (DIP; µmol L^{-1}) expressed in nitrogen-equivalent units relative to the Redfield ratio (**e**)

photons m^{-2} s^{-1} (DLI of 7.16 mol photons m^{-2} d^{-1}) in the unshaded, 15% and 30% shade treatments, respectively. Throughout the experiment, DIP (1.68 ± 0.51 µmol L^{-1}) and DIN (0.95 ± 0.65 µmol L^{-1}) varied (Fig. 1e). DIN remained relatively stable from 16–56 days (0.63 ± 0.24 µmol L^{-1}) but peaked at 1.8 µmol L^{-1} and 2.9 µmol L^{-1} at day 12 and 61, respectively.

Model behaviour under ambient conditions

The model simulated an expanding population in the ambient temperature treatment. Symbiont carbon reserves and symbiont population biomass increased throughout the 70-day model run (Fig. 2a, b, c). Symbiont carbon reserves remained relatively similar between the three shade scenarios at ambient temperature, increasing ~ 83-fold throughout the model run. Symbiont population biomass increased ~ 26- to 28-fold (all shade treatments). Thus, in the ambient scenario, the model simulated individual symbiont cells that are initially well-adjusted to the environmental conditions with stable symbiont photophysiology.

As consumption exceeded supply with increasing biomass, the symbiont's internal reserves of nitrogen and phosphorus decreased with cell division. Internal reserves remained relatively similar between the shade scenarios at ambient temperature (Fig. 2d, e, f). In the symbiont growth dynamics of the model, generating structural material for an additional cell requires the equivalent of 100% internal reserves of carbon, nitrogen, and phosphorus of one cell (Baird et al. 2018b). Internal nitrogen and phosphorus reserves show nutrients were moderately limiting; internal nitrogen decreased by ~ 0.34 to 0.39 (dimensionless), and internal phosphorus decreased by ~ 0.37 to 0.39 (dimensionless) (across all shade scenarios). Carbon fixation was not limited by temperature as the RuBisCO enzyme remained active under an ambient temperature scenario (Online resource 3: Fig. S1a), as demonstrated by the relatively stable internal carbon reserves (Fig. 2d, e, f). Nonetheless, due to the day/night cycle, energy reserves were depleted each night and returned to approximately half full during the day. Thus, the overall population increase was more limited by light than by nutrients.

An increasing quantity of the xanthophyll pigments (chlorophyll *a*, photosynthetic and photoprotective pigment concentration) was simulated (Fig. 2g, h, i). The symbiont's photosynthetic capability was not compromised; total chlorophyll *a* concentration increased ~ 28–32-fold (across all shade treatments). Rapid xanthophyll switching from photosynthetic to increased photoprotective pigment concentration between night and day was simulated with elevated irradiance during the doldrum events. Daily xanthophyll switching did not occur during reduced irradiance in the

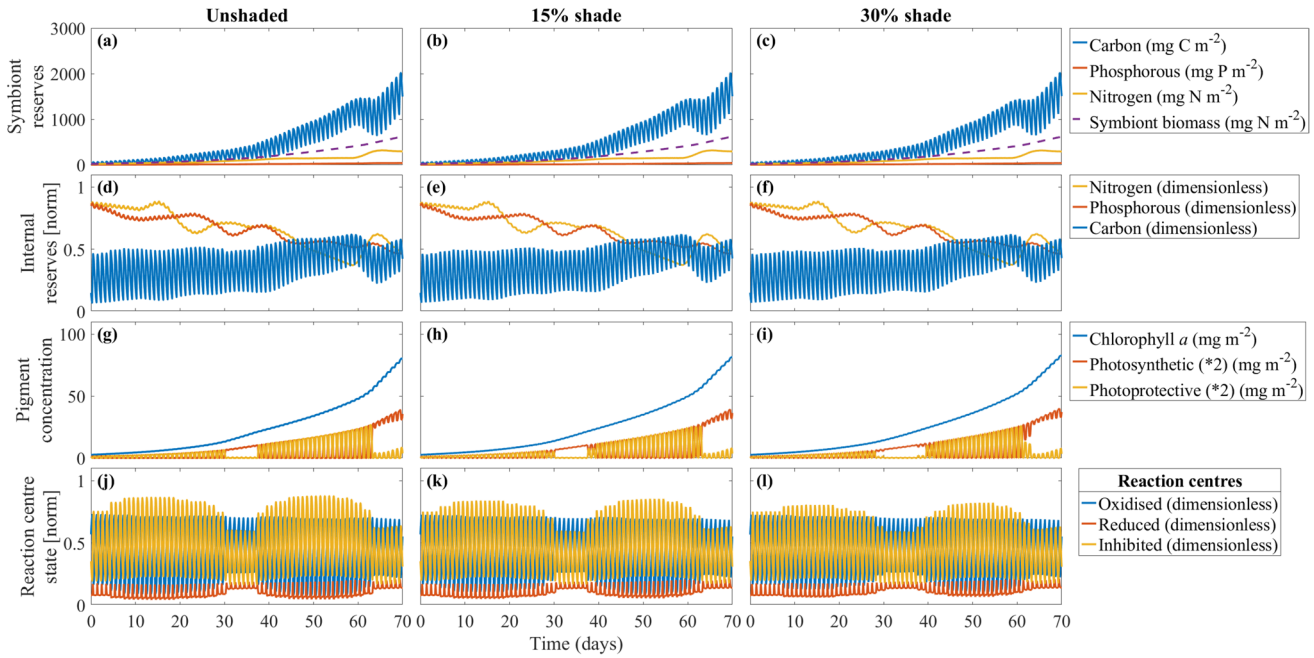

Fig. 2 Key model outputs for ambient temperature, unshaded (**a**, **d**, **g**, **j**), 15% shade (**b**, **e**, **h**, **k**), and 30% shade (**c**, **f**, **i**, **l**) scenarios: symbiont reserves (carbon, phosphorus, and nitrogen (mg m^{-2})) and symbiont biomass (mg N m^{-2}) (**a**, **b**, **c**), normalised internal reserves (nitrogen, phosphorus, and carbon (dimensionless)) (**d**, **e**, **f**), the concentration of chlorophyll *a* (mg m^{-2}) and photosynthetic and photoprotective xanthophyll pigments (mg m^{-2}) (**g**, **h**, **i**), and the normalised fraction of reaction centres in the state oxidised, reduced and inhibited (dimensionless) (**j**, **k**, **l**). Tick marks occur at 0:00 h

intermediate recovery period and the recovery post-doldrum two. Reduced xanthophyll switching occurred from 30–37 days (post-doldrum one) and 63–70 days (post-doldrum two) in the unshaded and 15% shade scenario (Fig. 2g, h). In the 30% shade treatment, the reduced switching rate was simulated for longer; the xanthophyll pigments were photosynthetic at 28–39 days and 61–70 days (Fig. 2i), and reaction centres were primarily oxidised (Fig. 2l). The reaction centres were inactive during the day, with recovery simulated overnight. As a result, the xanthophyll cycle was photoprotective mainly during the day and photosynthetic in the early morning.

The varying light reserves over a day influenced the fraction of reaction centres in the state oxidised, reduced, and inhibited (Fig. 2j, k, l). The fraction of inhibited reaction centres in the unshaded scenario (Fig. 2j) largely followed the downwelling light irradiance profile of the experiment (Fig. 1d). Oxidised reaction centres remained stable throughout the model run and peaked at ~ 74% of the total reaction centre concentration (across all shade treatments) (Fig. 2j, k, l). At 6 am, the reaction centres were highly oxidised (Online resource 4: Fig. S2j, k, l), all xanthophyll pigments were photosynthetic (Online resource 4: Fig. S2g, h, i), and the carbon reserves (both in the symbiont (Online resource 4: Fig. S2a, b, c) and internal reserves (Online resource 4: Fig. S2d, e, f)) were depleted. A high proportion of oxidised reaction centres before solar noon (Online resource 4: Fig. S2j, k, l) led to a peak in carbon reserves (symbiont (Online resource 4: Fig. S2a, b, c) and internal (Online resource 4: Fig. S2d, e, f)). At solar noon, reaction centres were highly inhibited (Online resource 4: Fig. S2j, k, l), and xanthophyll pigments were increasingly photoprotective (Online resource 4: Fig. S2g, h, i). The inhibited reaction centres were detoxified by the morning into oxidised reaction centres. Reaction centres were less inhibited with increased shade, peaking at ~ 78%, 76%, and 56% of the total reaction centre concentration, in the unshaded, 15% shade, and 30% shade scenario (Fig. 2j, k, l).

Model behaviour under heat stress conditions

Compared to the ambient temperature scenario, the model simulated a decline in coral photophysiological health and reduced symbiont population growth under heat stress. The simulated symbiont biomass and symbiont carbon and nitrogen reserves decreased between the moderate heat stress (Fig. 3) and high heat stress (Fig. 4) temperature scenarios. Symbiont reserves and biomass increased with increased shade in both heat stress scenarios (Fig. 3a, b, c, 4a, b, c). From day zero to the end of the simulation, symbiont population biomass increased by ~ 48%, 88% and 94% (unshaded, 15% shade, and 30% shade, respectively) in the moderate

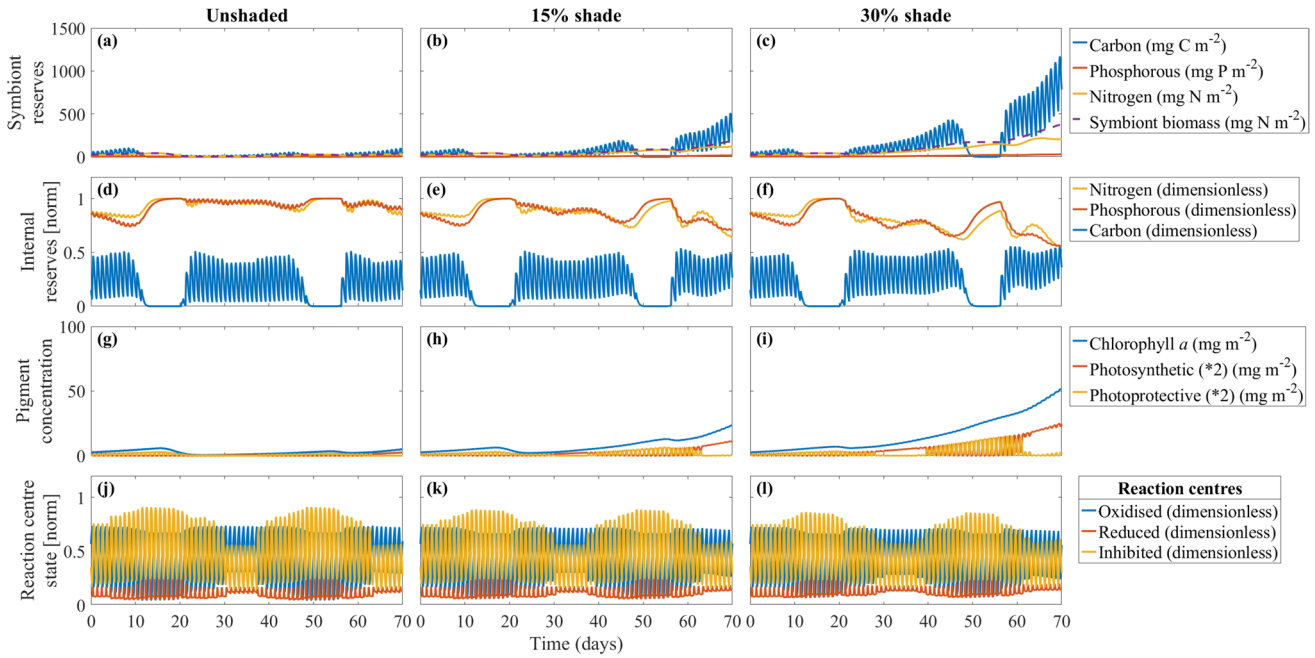

Fig. 3 Key model outputs for the moderate heat stress, unshaded (**a**, **d**, **g**, **j**), 15% shade (**b**, **e**, **h**, **k**), and 30% shade (**c**, **f**, **i**, **l**) scenarios: symbiont reserves (carbon, phosphorus, and nitrogen (mg m^{-2})) and symbiont biomass (mg N m^{-2}) (**a**, **b**, **c**), normalised internal reserves (nitrogen, phosphorus, and carbon (dimensionless)) (**d**, **e**, **f**), the concentration of chlorophyll *a* (mg m^{-2}) and photosynthetic and photoprotective xanthophyll pigments (mg m^{-2}) (**g**, **h**, **i**), and the normalised fraction of reaction centres in the state oxidised, reduced, and inhibited (dimensionless) (**j**, **k**, **l**). Tick marks occur at 0:00 h

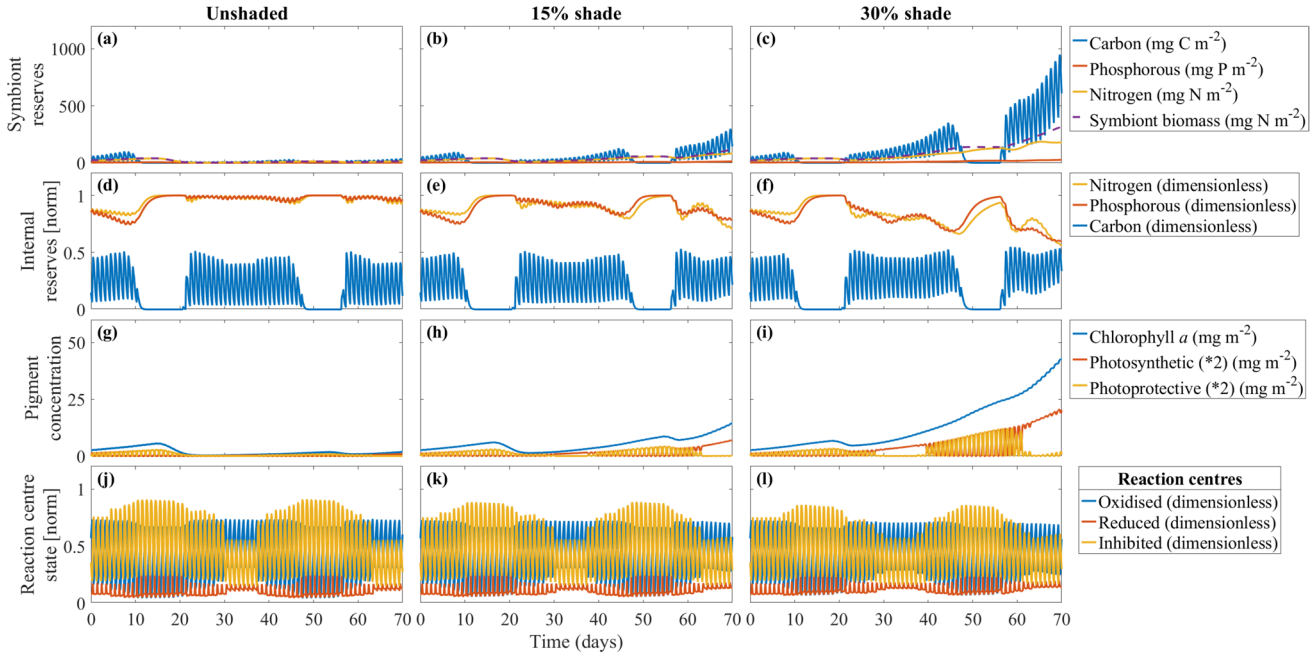

Fig. 4 Key model outputs for the high heat stress, unshaded (**a**, **d**, **g**, **j**), 15% shade (**b**, **e**, **h**, **k**), and 30% shade (**c**, **f**, **i**, **l**) scenarios: symbiont reserves (carbon, phosphorus, and nitrogen (mg m^{-2})) and symbiont biomass (mg N m^{-2}) (**a**, **b**, **c**), normalised internal reserves (nitrogen, phosphorus, and carbon (dimensionless)) (**d**, **e**, **f**), the concentration of chlorophyll *a* (mg m^{-2}) and photosynthetic and photoprotective xanthophyll pigments (mg m^{-2}) (**g**, **h**, **i**), and the fraction of reaction centres in the state oxidised, reduced, and inhibited (dimensionless) (**j**, **k**, **l**). Tick marks occur at 0:00 h

heat stress scenario. Symbiont biomass decreased by ~ 29% in the unshaded scenario and increased by ~ 81% and 93% in the 15% and 30% shade scenarios, respectively, under both heat stress scenarios.

In both heat stress temperature scenarios, carbon fixation was reduced by the temperature-inhibited RuBisCO enzyme (Online resource 3: Fig S1b, c). Reduced carbon fixation led to depleted internal carbon reserves during the doldrum events (Figs. 3d, e, f, 4d, e, f). Reduced internal carbon reserves limited symbiont population growth. Due to reduced symbiont growth, symbiont internal nitrogen and phosphorus reserves did not decline as low by the end of the model run in the heat stress scenarios (Figs. 3d, e, f, 4d, e, f) compared to the ambient temperature scenario (Fig. 2d, e, f). Internal nitrogen and phosphorus reserves were largely non-limited in the unshaded scenario at both heat stress scenarios and remained close to ~ 1 (dimensionless) after the first doldrum event (Fig. 3d, 4d). During reduced light levels in the intermediate recovery period and the recovery post-doldrum two, in the shaded scenarios, internal nitrogen and phosphorus reserves gradually declined with time (Figs. 3e, f, 4e, f), while symbiont biomass increased (Figs. 3b, c, 4b, c). In both heat stress scenarios, internal carbon reserves rapidly recovered in both the intermediate recovery period and the recovery post-doldrum two when light levels were reduced (Figs. 3d, e, f, 4d, e, f).

Pigment concentration was reduced with increased temperature and reduced shade (Figs. 3g, h, i, 4g, h, i). For instance, the end concentration of chlorophyll *a*, photosynthetic, and photoprotective pigments in the 30% shade scenario at moderate heat stress was ~ 32 mg m^{-2}, 10 mg m^{-2}, and 5 mg m^{-2}, compared to 5 mg m^{-2}, 2 mg m^{-2}, and 0.01 mg m^{-2} in the unshaded scenario at moderate heat stress. Rapid switching between photosynthetic and photoprotective pigment concentration was simulated during the doldrum events in all scenarios at heat stress (Figs. 3g, h, i, 4g, h, i). Xanthophyll pigments were photosynthetic at reduced light levels during the intermediate recovery period and in the recovery post-doldrum two. Xanthophyll pigment concentration increased under an increased shade level.

The proportion of oxidised, reduced, and inhibited reaction centres remained similar between the two heat stress scenarios (Figs. 3j, k, l, 4j, k, l) but varied between the ambient and heat stress scenarios. Greater inhibited reaction centres were simulated under heat stress. The proportion of inhibited reaction centres was only slightly reduced with increased shade. At moderate heat stress, inhibited reaction centres were 49%, 49%, and 48% (unshaded, 15% shade, and 30% shade, respectively) of the total reaction centre concentration. At high heat stress, inhibited reaction centres were 48%, 48%, and 47% (unshaded, 15% shade, and 30% shade, respectively) of the total reaction centre concentration.

During the doldrum events, fewer reaction centres were oxidised, and more reaction centres were reduced and inhibited in the heat stress scenarios.

Comparing simulated bleaching to the observed physiological response

The antioxidant activity and simulated bleaching were greatest under heat stress (Fig. 5). Symbiont cell expulsion was simulated only in the heat stress scenarios (moderate and high). On day 54, the antioxidant activity of CAT and SOD was greatest in the moderate heat stress treatment (39.75 ± 18.03, and 175.63 ± 53.11 U mg^{-1} protein, respectively; $P < 0.05$ and $P < 0.01$, respectively; Online resource 1: Table S1) (Fig. 5e, f). On day 54, in the unshaded treatment, SOD was greatest in the moderate heat stress treatment (222.84 ± 55.67 U mg^{-1} protein; $P < 0.05$) (Fig. 5h). On days 40 and 68, SOD was greatest in the high heat stress treatment (126.69 ± 37.52, and 106.03 ± 39.86 U mg^{-1} protein, respectively; $P < 0.01$) (Fig. 5i). On day 19, SOD was lowest in the ambient temperature treatment (92.60 ± 32.78 U mg^{-1} protein; $P < 0.01$) (Fig. 5g). At day 54, SOD under 30% shade treatment was greater in the high heat stress treatment (147.89 ± 40.21 U mg^{-1} protein) (Fig. 5i) than in the ambient temperature treatment (67.35 ± 17.84 U mg^{-1} protein; $P < 0.05$) (Fig. 5g).

The antioxidant activity and simulated bleaching were reduced with increased shade (Fig. 5). On day 19, CAT was the most reduced in the 30% shade treatment, compared to CAT in the other shade treatments, for all temperature treatments (28.32 ± 10.77 U mg^{-1} protein; $P < 0.01$) (Fig. 5d, e, f). On day 19, SOD was greatest in the unshaded treatment, compared to SOD in the other shade treatments, for all temperature treatments (153.67 ± 49.08 U mg^{-1} protein, $P < 0.01$) (Fig. 5g, h, i). On day 40, SOD was greatest in the unshaded treatment, compared to SOD in the other shade treatments, for all temperature treatments (127.53 ± 41.07 U mg^{-1} protein, $P < 0.01$) (Fig. 5g, h, i). On day 54, SOD was the most reduced in the 30% shade treatment, compared to SOD in the other shade treatments, for all temperature treatments (116.66 ± 48.29 U mg^{-1} protein, $P < 0.01$) (Fig. 5g, h, i). On day 68, CAT was greatest in the unshaded treatment, compared to CAT in the other shade treatments, for all temperature treatments (31.92 ± 14.31 U mg^{-1} protein; $P < 0.01$; Online resource 1: Table S1) (Fig. 5d, e, f).

The antioxidant activity increased from the first to the second sampling time in all treatments (Fig. 5). In both heat stress treatments, this increased activity occurred over the first doldrum event. The first doldrum event coincided with a peak in ROS concentration above the threshold, triggering symbiont cell expulsion (Fig. 5b, c). The antioxidant activity also increased between the first and second

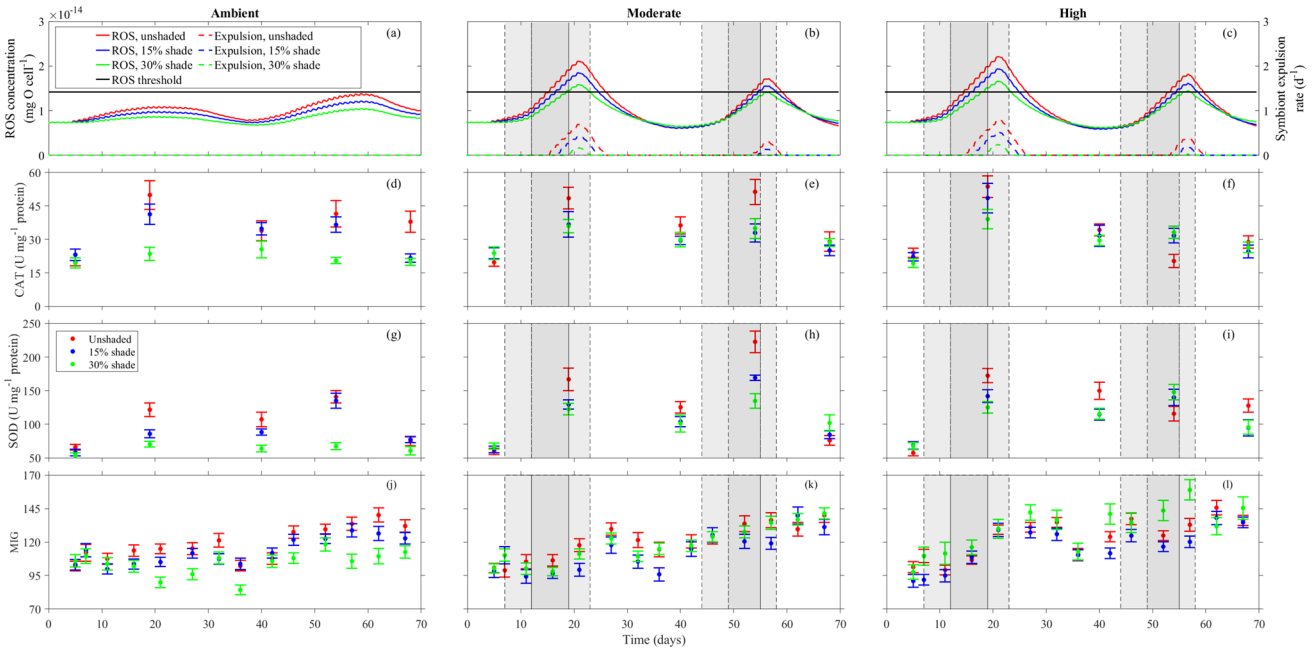

Fig. 5 Simulated ROS concentration ($\times 10^{-14}$ mg O cell^{-1}), ROS threshold (1.42×10^{-14} mg O cell^{-1}), normalised symbiont expulsion rate (d^{-1}) (**a**, **b**, **c**) in comparison with observed catalase activity (CAT; U mg^{-1} protein) (**d**, **e**, **f**), superoxide dismutase activity (SOD; U mg^{-1} protein) (**g**, **h**, **i**), and the mean intensity of grey (MIG) (**j**, **k**, **l**) for the ambient temperature, moderate heat stress, and high heat stress treatments, in the unshaded, 15%, and 30% shade treatments, averaged ± standard error, recorded for *Acropora kenti*. The grey regions represent the two doldrum events emulated in the marine heatwave experiment, consisting of a temperature ramp-up period, a doldrum period, and a temperature ramp-down period

sampling points in the ambient temperature treatment; simulated ROS concentration increased over the first doldrum event but did not exceed the ROS threshold (Fig. 5a). In the ambient temperature treatment, the irradiance levels were increased during the doldrum periods without an increase in temperature. Both antioxidant activity and ROS concentration responded to the increased light levels of the doldrum periods. A decline in antioxidant activity was observed at the third sampling event, which was towards the end of the intermediate recovery period; ROS concentration declined to a minimum level during this period of reduced light and heat stress or just reduced light stress (ambient temperature scenario). Over the second doldrum event, increased antioxidant activity was observed mostly for SOD in the unshaded and 15% shade treatment at ambient temperature (Fig. 5g) and moderate heat stress (Fig. 5h), and for CAT in the unshaded treatment at moderate heat stress (Fig. 5e).

Across the treatments, 64% of the variation in CAT activity was captured by SOD activity ($F_{(1, 43)} = 74.82$, $P < 0.001$, $r^2 = 0.64$) (Fig. 6a). The regression between antioxidant activity and simulated ROS concentration was also statistically significant (CAT: $F_{(1, 43)} = 42.78$, $P < 0.001$, $r^2 = 0.50$; SOD: $F_{(1, 43)} = 33.39$, $P < 0.001$, $r^2 = 0.44$) (Fig. 6b, c). Antioxidant activity measurements taken outside the doldrum periods were generally lower in value, matched by lower simulated ROS concentration (Fig. 6b, c). For the antioxidant values below the regression line, the simulated ROS concentration was lower than predicted by the regression model. Antioxidant activity measurements taken inside the doldrum periods (marked by '*x*' in Fig. 6) were generally higher in value and were matched by higher simulated ROS concentration. For the antioxidant values above the regression line, the simulated ROS concentration was higher than predicted by the regression model.

Comparing simulated bleaching to the observed visual response

Overall, the trends in MIG (Fig. 5j, k, l) agreed well with the pattern of stress–recovery–stress simulated by the model (Fig. 5a, b, c). The shade effects were consistent across temperature scenarios in the model but not across treatments in the experiment. MIG appeared reduced under a higher shade level at ambient temperatures (Fig. 5j); however, under high heat stress, MIG appeared greater under a higher shade level (Fig. 5l). Shade and temperature as fixed factors alone did not affect the multivariate response of MIG ($P < 0.05$; Online resource 2: Table S2). The dominant sources of variation in the MIG data were tank (nested in temp x shade), time, the interaction between temperature and time (temp × time), and the three-way interaction between shade, temperature, and

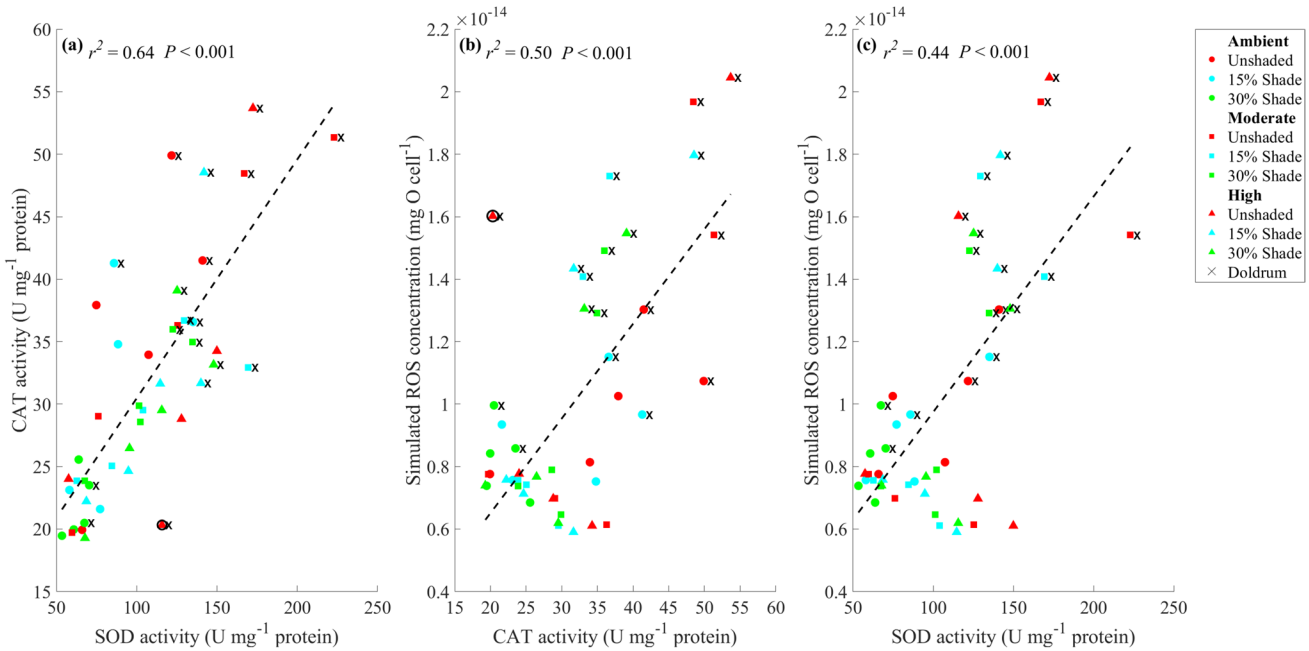

Fig. 6 Regression scatterplot of superoxide dismutase activity (SOD; U mg^{-1} protein) against catalase activity (CAT; U mg^{-1} protein) (**a**), catalase activity (CAT; U mg^{-1} protein) against simulated ROS concentration (×10^{-14} mg O cell^{-1}) (**b**) and superoxide dismutase activity (SOD; U mg^{-1} protein) against simulated ROS concentration (×10^{-14} mg O cell^{-1}) (**c**) for all treatments, recorded for *Acropora kenti*. For the antioxidant data, each point represents an average of SOD or CAT activity. The circled anomalous values on (**a**) and (**b**) were removed from the regression analysis of (**a**) and (**b**) only. Crosses (X) indicate samples taken inside the doldrum events (this includes samples from the ambient temperature treatment that experienced increased light levels)

time (shade × temp × time) ($P < 0.001$; Online resource 2: Table S2).

MIG varied over time ($P < 0.001$), and this temporal variation was strongly influenced by both shade and temperature treatments (shade × temp × time; $P < 0.001$). Under high heat stress and no shade, MIG showed the most pronounced and rapid changes, with significant differences emerging early (days 5–21: t = 5.51, $P = 0.0001$) and persisting across time points (days 5–67: $t = 6.34$, $P = 0.0001$). In contrast, under high heat stress with 30% shade, changes in MIG were less significant (days 5–21: $t = 3.62$, $P = 0.0009$; days 5–67: $t = 4.87$, $P = 0.0001$). These results highlight that the trajectory of MIG over time is highly context-dependent, shaped by the combined effects of heat and light environments.

The overall trend of MIG largely followed the simulated ROS concentration (Fig. 5). MIG increased over time under most shade and temperature treatments, and both MIG and ROS concentrations increased around the first and second doldrum events and declined during the intermediate recovery period. Under ambient temperatures, MIG was greater over the second doldrum period (Fig. 5j), consistent with the simulated ROS concentration for the ambient scenario (Fig. 5a). However, under heat stress, ROS concentration and symbiont cell expulsion were greater over the first doldrum event (Fig. 5b, c).

Most increases in MIG began on day 21, during the ramp-down period of the first doldrum event, and MIG continued to increase into the intermediate recovery period (Fig. 5). On day 21, ROS reached a peak concentration in all temperature scenarios, and the symbiont cell expulsion rate peaked in both heat stress scenarios. However, fewer increases in MIG were observed from day 5 to day 36; the MIG appeared to recover (a decreased MIG) with subsequent samples taken in the intermediate recovery period. The simulated ROS concentration declined from the ramp-down period of the first doldrum event to the start of the second doldrum event.

The interaction between temperature and time was significant (temp × time; $P < 0.001$), indicating that the effect of time on MIG varied by the temperature treatment. In the ambient temperature treatment, significant differences emerged primarily between early (days 5 and 7) and later time points (days 46–67), with p values often < 0.001. In the high heat stress temperature treatment, the temporal differences in MIG were even more pronounced, with many differences in MIG between early and later time points (for instance, day 5 vs. days 21–67) demonstrating high significance ($P = 0.0001$). A similar pattern was observed in the moderate heat stress temperature treatment, though the magnitude of change in MIG appeared less extreme than under high heat stress. These results demonstrated that the temporal dynamics in MIG were inconsistent across temperature treatments, with greater divergence over time under high heat stress temperatures.

The significant tank(temp x shade) result ($P < 0.001$), as revealed by the PERMDISP analysis ($P = 0.0001$), indicated that the multivariate dispersion was not uniform across tanks, and that the interaction between temperature and shade treatments influenced this variability. Tank 25 (high heat stress temperature treatment, 15% shade) had the highest average distance to centroid (1.06), indicating greater variability in that tank. Tank 11 (ambient temperature treatment, 15% shade), by contrast, had the lowest dispersion (0.54), indicating the MIG results from this tank had a more homogeneous response under those conditions.

Comparing simulated and observed photochemistry

The overall trends in observed F_v/F_m agreed well with the pattern of stress–recovery–stress of simulated F_v / F_m (Fig. 7). Overall, the simulated F_v/F_m displayed a minimal decline; F_v/F_m decreased by only ~ 0.01 to 0.05 in all scenarios. Simulated F_v/F_m remained most similar between shade levels in the ambient temperature scenario (0.70 ± 0.02 in all shade scenarios) (Fig. 7a, b, c). However, the simulated F_v/F_m at heat stress (Fig. 7d–i) displayed substantial drops in value during the doldrum period of both doldrum events. The simulated F_v/F_m recovered in value with a decrease in both light and temperature during the ramp-down period of each doldrum event.

Minimal simulated differences in F_v/F_m were shown between the shade scenarios (Fig. 7), and shade had no significant effect on the observed F_v/F_m ($P > 0.05$; Online resource 2: Table S2). Time was the only fixed factor with a strong and significant effect on observed F_v/F_m ($P < 0.001$), suggesting that F_v/F_m changed over time in the experiment. Many time points differed, for instance, days 7 and 11 differed from almost all later time points (days 21–67), with very low p values (often $P = 0.0001$). This suggests a strong temporal shift in F_v/F_m values throughout the experiment. The magnitude of t-values increased as the time gap widened (for instance, day 7 versus day 52 had a t-value of 15.12; this indicated a gradual and consistent change in F_v/F_m, rather than abrupt fluctuations. Comparisons among later sampling times (for instance, day 52 vs. day 57, and day 62 vs. day 67) were mostly non-significant ($P > 0.05$), suggesting a plateau or stabilisation in F_v/F_m values.

The significant tank(temp × shade) result ($P < 0.001$), as revealed by the PERMDISP analysis ($P = 0.0001$), indicated that the multivariate dispersion was not uniform across tanks, and that the interaction between temperature and shade treatments influenced this variability. Tank 4 had a higher dispersion (1.26), suggesting that this tank had much more variability than the others.

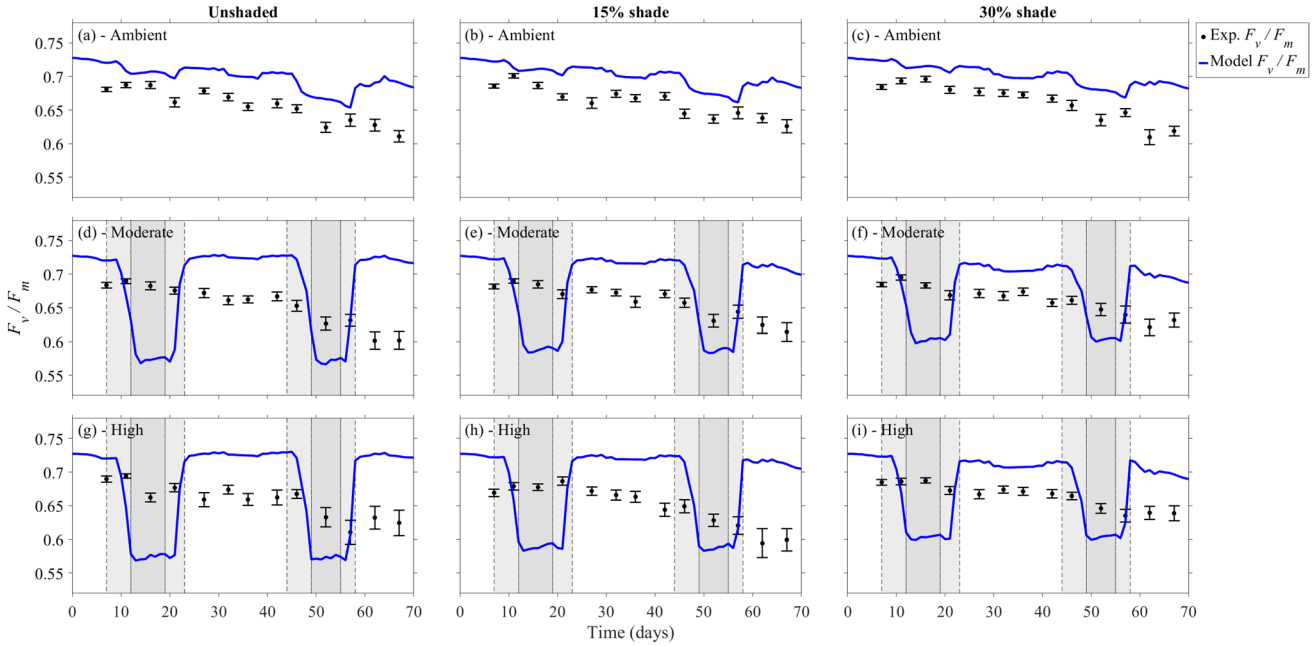

Fig. 7 Observed F_v/F_m against simulated F_v/F_m for the ambient temperature, moderate heat stress, and high heat stress treatments, in the unshaded, 15%, and 30% shade treatments, averaged ± standard error, recorded for *Acropora kenti.* The grey regions represent the two doldrum events emulated in the marine heatwave experiment, consisting of a temperature ramp-up period, a doldrum period, and a temperature ramp-down period

Comparing simulated bleaching to fragment removals

The model simulated bleaching stress and bleaching to be consistently reduced with an increased shade level or greater with an increased temperature scenario. Similarly, the total number of fragment removals per tank (day 70) was reduced under moderate heat stress (92 removals), in comparison with the ambient temperature (155) or high heat stress (174) scenarios ($P < 0.01$, Online resource 1: Table S1). No differences in the total number of fragment removals (day 70) per tank were observed between the shade scenarios ($P > 0.05$, Online resource 1: Table S1). However, the overall trend of fragment removals (Fig. 8, dotted lines) agreed well with reduced bleaching (symbiont cell expulsion rate) simulated in scenarios of increased shade (Fig. 8, dashed lines).

Shade had mixed effects on the onset of fragment removal. In the ambient temperature (Fig. 8a) and high heat stress treatments (Fig. 8c), removals began on day 34 across all shade levels. In the moderate heat stress treatment (Fig. 8b), the onset of removal varied by shade level: day 37 in the unshaded treatment, day 34 in the 15% shade treatment, and day 50 in the 30% shade treatment. Removals started during the intermediate recovery phase for all treatments except the moderate heat stress with 30% shade. In that specific treatment, removals began later during the second doldrum period.

Discussion

Models are assessed by their degree of 'model fit', and how well the model results fit observation-based data determines model accuracy (Baumberger et al. 2017). Here, we build on the previous validation of the coral bleaching model (Ellis et al. 2025b). We evaluated whether model outputs adequately represented the target species (*Acropora kenti*) under an emulated multi-doldrum marine heatwave event. The overall trends in the observed state of *A. kenti* agreed well with the pattern of stress–recovery–stress simulated by the model, and the simulated bleaching stress captured up to fifty per cent of the variation in observed antioxidant enzyme activity. Overall, the model adequately represented bleaching outcomes concerning the interactions between temperature and light.

The model configuration may not be adequately light sensitive to represent the bleaching of *A. kenti* under ambient temperatures. The observed bleaching was likely due to elevated ambient light levels in the experiment exceeding what the fragments were acclimatised to. The model simulated bleaching stress for the ambient scenario but no symbiont cell expulsion, thus contrasting with the relatively higher number of fragment removals for the ambient temperature treatment. To achieve greater light sensitivity in simulations, the model could be configured with fewer photons that lead to the generation of ROS (parameter = m_{P2R}). We

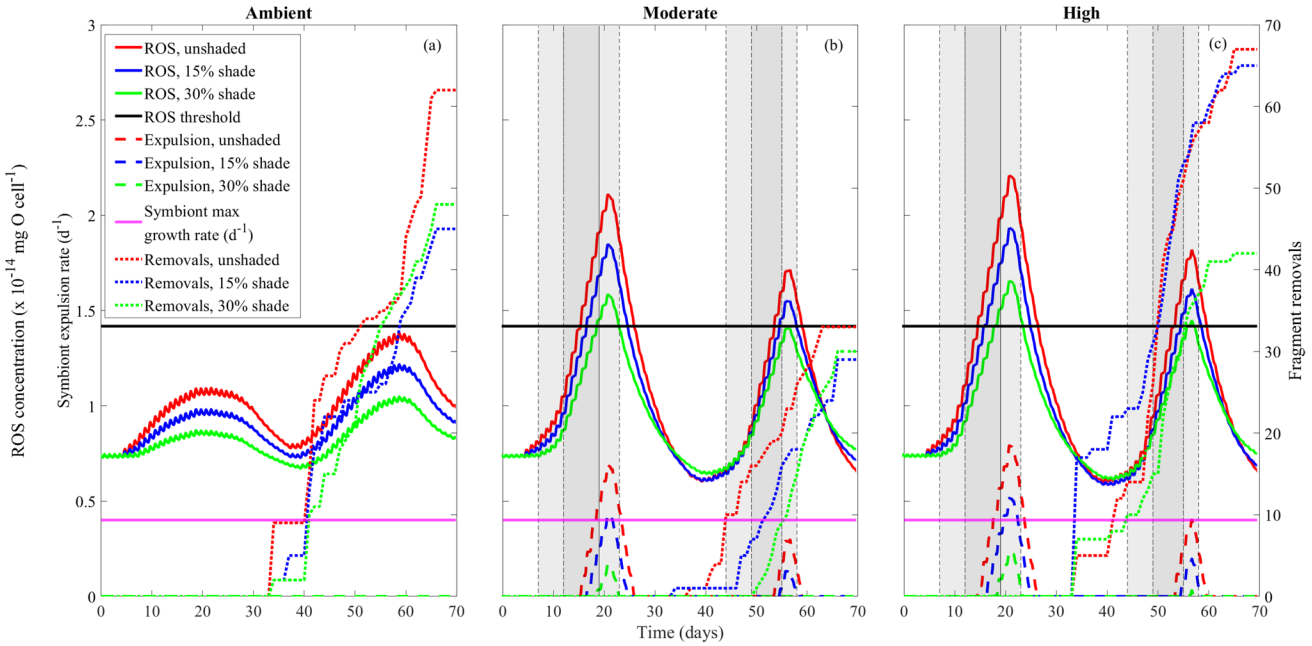

Fig. 8 Simulated ROS concentration ($\times 10^{-14}$ mg O cell^{-1}), ROS threshold (1.42×10^{-14} mg O cell^{-1}), normalised symbiont expulsion rate (d^{-1}), and symbiont maximum growth rate (d^{-1}) in the ambient temperature (**a**), moderate heat stress (**b**), and high heat stress (**c**) scenarios, for the unshaded, 15%, and 30% shade scenarios, in comparison with the cumulative number of fragment removals by treatment. The grey regions represent the two doldrum events simulated in the marine heatwave experiment, consisting of a temperature ramp-up period, the doldrum period, and the temperature ramp-down period

recommend quantifying the amount of light absorbed by an inhibited reaction centre that generates ROS and considering how this varies between coral species. We refer to another mechanistic model of coral bleaching that uses two values of excess light leading to ROS production, one for a 'tolerant' and a 'sensitive' symbiont species (Brown et al. 2022). Determining bleaching susceptibility, for example, the ability to repair photodamage caused by light stress (Ragni et al. 2010), could be achieved by measuring photoinhibition, generally defined as the light-induced loss of oxygen evolution and electron-transport activity of PSII (Tyystjärvi 2013). Incorporating the light sensitivity of different coral species into the modelling approach could improve simulated bleaching under varying environmental conditions.

Predicting the onset and accumulation of coral bleaching stress

The mechanisms controlling antioxidant enzyme activity and MIG represent different pathologies in the coral bleaching process. Increased antioxidant activity is likely due to accumulated ROS levels (Lesser 2010); MIG is a secondary bleaching effect resulting from longer-term exposure to heat stress and elevated light (Hoegh-Guldberg and Smith 1989; Jones 1997). The degree of chlorophyll pigmentation in the symbiont is influenced by processes independent of ROS concentration, which may explain the delayed peak in observed MIG. In both experimental doldrum events, the light increased before temperature increases and persisted at higher values after the temperature had returned to ambient, exposing *A. kenti* to sustained elevated light. The pre-doldrum light levels were also higher than the light levels in the intermediate recovery period and the recovery period post-doldrum two. This prolonged light exposure likely contributed to the lag in observed MIG. Consequently, comparing an observed physical bleaching response to simulated physiological bleaching may not be a good measure of model fit, as was evident in this study. Thus, MIG may not be a recommended proxy for validating photophysiological models of coral bleaching.

Overall, the health of *A. kenti* declined under experimental conditions of increased light and temperature, aligning with the simulated bleaching. Interestingly, while statistical analysis revealed no significant differences in MIG across shade levels when shade was treated as a fixed factor, some patterns suggested a potential benefit of shade under ambient temperature conditions. Specifically, MIG appeared lower under higher shade levels at ambient temperatures. However, under high heat stress, this trend was not observed; in fact, MIG was highest in the 30% shade treatment, suggesting that the protective effect of shade may diminish or even reverse under accumulated heat stress. These observations, though not statistically significant, highlight the complexity of shade interactions

under varying thermal regimes. It is possible that the MIG method was influenced by subtle lighting variations that were not fully corrected by the colour calibration card. Additional factors such as tank position, coral fragment placement, and camera model may have introduced variability. Future studies could consider imaging corals in a controlled, independent tank environment to enhance the reliability of the MIG method. However, care must be taken to account for potential confounding effects such as sampling time and handling stress.

The benefits of shading corals have been shown to decline with accumulated heat stress. Shading delayed bleaching up to 3 °C-weeks in *Duncanopsammia axifuga*, but this species was unresponsive to shading when 3 °C-weeks was surpassed (Butcherine et al. 2023). In another experiment, shade was effective under intense light conditions up to 4 °C-weeks, with reduced protection up to 8 °C-weeks (Coelho et al. 2017). Persistent low light levels can significantly impact growth (Comeau et al. 2014). For instance, low survival and recruitment were demonstrated for corals underneath the shade of large *Acropora hyacinthus* colonies (Baird and Hughes 2000). Similarly, both an unshaded treatment and the treatment of the greatest shade (87% shade) were found to have the largest reduction in symbiont density (Piggot et al. 2009). Reduced irradiance under shade application does not necessarily benefit all corals equally; *Acropora kenti* has demonstrated a prior negative response to shade under heat stress conditions (Ellis et al. 2024), which corresponds with the observed trends of this study. In Ellis et al. (2024), shading did not reduce the effects of bleaching in *A. kenti*; the MIG was greatest in the shaded treatment. These findings suggest that shade effects during heat stress conditions are not uniform, potentially due to complex photosynthetic pathways and differences in tolerances between coral species and their symbionts. Further research is required to disentangle the role of shade in reducing bleaching at increased heat stress.

Symbiont species have shown a strong effect on bleaching susceptibility (Cunning et al. 2015; Silverstein et al. 2017), with 'tolerant' symbionts able to repair photodamage caused by light stress (Ragni et al. 2010) or have a stable photosynthetic apparatus (Tchernov et al. 2004). However, theoretical models incorporating within-host dynamics of multiple symbionts rely on assumptions. Quantitative models, including physiological rates that control within-coral host–symbiont interactions, have become available through Dynamic Energy Budget models (Cunning et al. 2017; Eynaud et al. 2011; Muller et al. 2009). A recent analysis of a mechanistic model found that including a tolerant symbiont can increase host survival and recovery (Brown et al. 2022). Representing a coral in symbiosis with multiple symbiont species, thus including varying light tolerances, may enable better predictions of coral bleaching.

The increased light and temperature treatments did not significantly affect the photochemical health of *A. kenti,* despite a physiological and visual decline being observed. High temperatures and elevated light intensities are known to increase ROS production in host tissues and symbionts, as shown by increased antioxidant activity (Higuchi et al. 2015). Elevated temperatures also lower the threshold for photoinhibition, and a decreased F_v/F_m ratio indicates damage to photosystem II of the symbiont (Bhagooli and Hidaka 2004a). However, our observed F_v/F_m remained unaffected, suggesting that *A. kenti*'s photosystem was undamaged. Certain environmental stressors can impact the coral host and symbiont through multiple cascades, similarly, many mechanisms can produce ROS, and bleaching has occurred independently of oxidative stress (Helgoe et al. 2024). We suggest that the observed bleaching and resulting number of removals for *A. kenti* occurred due to oxidative stress rather than a decline in photosynthetic efficiency, highlighting the complexity of the coral bleaching response.

Discrepancies between F_v/F_m and visual bleaching responses are not uncommon (Castro-Sanguino et al. 2024; Jeans et al. 2014). Bleached coral tissues can retain symbionts with quantum yields comparable to unbleached corals (Fitt et al. 2001; Jones et al. 2000). Our experiment measured proxies of coral bleaching from different origins: photochemical health of the symbiont (F_v/F_m), visual health of the coral holobiont (MIG), and physiological health of the coral holobiont (antioxidant enzyme activity of SOD and CAT). Our results show that coral host health declined over time under heat and light stress, as evidenced by increased MIG, antioxidant activity, and the number of removals, while the symbiont's photochemistry remained unchanged. This is consistent with findings by Bhagooli and Hidaka (2004b), who reported no significant differences in photosystem II functioning or overall photosynthesis between retained and expelled symbionts following high-temperature stress. Therefore, photochemical changes may not be consistent with other proxies of bleaching, and temperature and light may induce different pathologies during coral bleaching. However, previous validation of the CBM for a different coral species, *Acropora divaricata*, demonstrated good agreement between the onset of simulated bleaching and a significant decline in photochemistry (Ellis et al. 2025b). This underscores the importance of selecting a bleaching proxy specific to the research question.

Predicting an intermediate recovery in light and heat stress

The model simulations and observed physiological, visual, and photochemical proxies demonstrated an intermediate recovery in bleaching stress between the doldrum events. However, the model may face difficulty resolving the

accumulation of heat and light stress experienced by corals *ex situ*. Notably, more bleaching stress was simulated during the first doldrum event, whereas the observed bleaching response was generally greater during the second doldrum event. We propose that more bleaching stress was simulated over the first event due to the increased light levels that preceded it. When the experimental light was dropped to its lowest level, in the intermediate recovery period, the bleaching was simulated at its lowest. This temporary recovery resulted in less bleaching stress simulated during the second doldrum event. *A. kenti's* simulated recovery may have been overpredicted. The simulated bleaching stress continued to decline up to the start of the second doldrum event. However, under the experiment's heat stress conditions, antioxidant activity and MIG did not recover to initial levels, indicating that a full recovery in coral health was not achieved. If the model simulated less recovery in bleaching stress, it may have better aligned with the observed pattern of greater bleaching stress during the second doldrum event. Corals in situ may accumulate bleaching stress over extended periods, preventing such recovery. Thus, further work may be required to ensure the pattern of stress and recovery simulated by the model over a marine heatwave event is representative of conditions in the natural reef environment. We suggest the discrepancy between the simulated and observed bleaching could be linked to the model's representation of ROS detoxification. Reducing the rate of ROS detoxification may slow the recovery rate, thus increasing the bleaching stress simulated over the second doldrum event.

Considerations

The analysis of CAT and SOD activity indirectly informs of ROS presence in the coral holobiont. Antioxidant activity was specific to neither the host nor the symbiont. Thus, increased total antioxidant activity could relate to increased ROS levels from within the symbiont or coral host or a combination of both entities. The CBM's simulated bleaching stress is based on intracellular ROS. Consequently, the observed and simulated antioxidant activity could relate to ROS sourced from different sites. In the current configuration, we removed the coefficient that accounts for the loss of intracellular ROS to extracellular pools (Ellis et al. 2025b). A fitted parameter should be included in the model for the ROS loss coefficient based on experimental evidence. We recommend quantifying the amount of ROS that moves from intracellular to extracellular pools under ambient and heat and light stress conditions.

Under ambient temperature conditions, coral bleaching was observed, and fragments were subsequently removed; the model simulated only bleaching stress for this scenario and no bleaching (symbiont cell expulsion). Light stress was observed in the ambient scenario, and a greater shade level reduced simulated bleaching. However, for the model to represent the observed response in the ambient temperature treatment, we would expect bleaching to be simulated for this scenario. The discrepancy between the observed and simulated response at ambient temperature may be explained by factors that the model cannot represent, for example, handling stress or the contamination of external light leaked from other treatments, with handling effects highlighted in previous studies and avoided where possible (Lesser 1997; Middlebrook et al. 2008).

Including tank as a random nested factor was essential to account for variability among replicate tanks that could influence coral responses independently of the fixed treatment effects. This statistical design incorporates the effect of microenvironmental differences within the controlled experimental setup, namely subtle variations in water flow, light diffusion, or microbial communities. Significant tank effects were demonstrated in the statistical analyses, along with significant dispersion detected by PERMDISP in some cases, indicating that differences in central tendency and variability among tanks contributed to the observed responses. These findings underscore the complexity of ex situ coral experiments. To reduce tank effects in future studies, researchers might consider rotating coral fragments and taking steps to minimise light leakage between adjacent tanks with different light treatments.

Conclusions

Using a previously validated configuration of the CBM, we studied the response of *A. kenti* over a theorised marine heatwave and doldrum-driven bleaching episode. The antioxidant enzyme activity observed in the experiment captured up to fifty per cent of the variation in ROS-induced bleaching stress simulated by the model. The predictive skill demonstrated by the CBM confirmed that the model's significant emergent features were present specifically that the model can simulate realistic amounts of cell expulsion under various light and temperature scenarios.

The degree of model fit between the observed and simulated bleaching response varied by the experimental bleaching proxy measured. *A. kenti*'s response to shade in the high heat stress treatment corresponded with previous bleaching results for this species. The impact of light was underrepresented by the model in the ambient temperature treatment when evaluated against MIG, while the observed photochemical response of *A. kenti* was unimpacted by light or temperature treatment.

We make recommendations for future model refinement, contingent upon quantitative data provided from experimental trials. These include adjusting the number of photons required to generate ROS, including a fitted parameter for

the ROS coefficient grounded in experimental measurements, and revisiting the ROS detoxification rate to more accurately reflect stress and recovery dynamics observed in the natural environment.

We recognise there is still a need for further research to explore the nuanced role of shade in reducing bleaching under elevated heat stress. Numerical modelling can represent shading management strategies and optimise future initiatives for deployment. Using the CBM to represent previous coral bleaching episodes could help determine the relative role of environmental stressors in future bleaching events.

Acknowledgements The authors would like to acknowledge the Traditional Owners of the Gumbaynggirr country where this study was conducted and all Traditional Owners of the Great Barrier Reef and its Catchments as First Nations Peoples who hold the hopes, dreams, traditions, and cultures of the Reef. We thank David Hughes, Matt Salmon, Shanae Read, and the research technicians at the National Sea Simulator facility, Australian Institute of Marine Science, for their experimental assistance.

Author contributions SE, DH, and KS contributed to conceptualisation. PB, SE, and CH were involved in experimental design. SE, CH, PB, and AF contributed to collection of experimental data and were involved in processing of experimental data. SE was involved in statistical analysis and writing—original draft preparation. MB, LH, and SE contributed to model configuration. DH was involved in funding acquisition and supervision. All authors commented on previous versions of the manuscript. All authors read and approved the final manuscript.

Funding Open Access funding enabled and organized by CAUL and its Member Institutions. The Reef Restoration and Adaptation Program is funded by the partnership between the Australian Government's Reef Trust and the Great Barrier Reef Foundation.

Data availability The experimental environmental data and validation data (experimental_data.xlsx) and simulated outputs from the CBM (model_data) used in this study are available for download from GitHub (Ellis et al. 2025a).

Code availability The code to run the CBM (Bleach_SCU_lab_exp_2024.m and Run_Bleach_SCU_lab_exp_2024.m) is available on GitHub, in the 'main' branch of the 'coral-bleaching-model' repository (Baird et al. 2024).

Declarations

Conflict of interest The authors declare no competing interests.

References

AIMS (2020) Northern Australia Automated Marine Weather and Oceanographic Stations, Sites: [Davies Reef]. https://doi.org/10.25845/5c09bf93f315d

Anderson MJ (2017) Permutational Multivariate Analysis of Variance (PERMANOVA). In Balakrishnan N, Colton T, Everitt B, Piegorsch W, Ruggeri F, Teugels JL (Eds.), Wiley StatsRef: Statistics Reference Online (pp. 1–15). John Wiley & Sons, Ltd. https://doi.org/10.1002/9781118445112.stat07841

Anthony KRN, Hoogenboom MO, Connolly SR (2005) Adaptive variation in coral geometry and the optimization of internal colony light climates. Funct Ecol 19:17–26. https://doi.org/10.1111/j.0269-8463.2005.00925.x

Baird AH, Hughes TP (2000) Competitive dominance by tabular corals: an experimental analysis of recruitment and survival of understorey assemblages. J Exp Mar Biol Ecol 251:117–132. https://doi.org/10.1016/S0022-0981(00)00209-4

Baird ME, Walker SJ, Wallace BB, Webster IT, Parslow JS (2003) The use of mechanistic descriptions of algal growth and zooplankton grazing in an estuarine eutrophication model. Estuar Coast Shelf Sci 56:685–695. https://doi.org/10.1016/S0272-7714(02)00219-6

Baird AH, Madin JS, Álvarez-Noriega M, Fontoura L, Kerry JT, Kuo CY, Precoda K, Torres-Pulliza D, Woods RM, Zawada KJA, Hughes TP (2018a) A decline in bleaching suggests that depth can provide a refuge from global warming in most coral taxa. Mar Ecol Prog Ser 603:257–264. https://doi.org/10.3354/meps12732

Baird ME, Mongin M, Rizwi F, Bay LK, Cantin NE, Soja-Woźniak M, Skerratt J (2018b) A mechanistic model of coral bleaching due to temperature-mediated light-driven reactive oxygen build-up in zooxanthellae. Ecol Model 386:20–37. https://doi.org/10.1016/j.ecolmodel.2018.07.013

Baird ME, Mongin M, Rizwi F, Bay LK, Cantin NE, Morris LA, Skerratt J (2021) The effect of natural and anthropogenic nutrient and sediment loads on coral oxidative stress on runoff-exposed reefs. Mar Pollut Bull 168:1–18. https://doi.org/10.1016/j.marpolbul.2021.112409

Baird ME, Jørgensen JT, Harrison L, Ellis SL (2024) Coral Bleaching Model [Matlab]. https://github.com/gbrrestoration/coral-bleaching-model

Baker AC, Glynn PW, Riegl B (2008) Climate change and coral reef bleaching: an ecological assessment of long-term impacts, recovery trends and future outlook. Estuar Coast Shelf Sci 80:435–471. https://doi.org/10.1016/j.ecss.2008.09.003

Baumberger C, Knutti R, Hirsch Hadorn G (2017) Building confidence in climate model projections: an analysis of inferences from fit. Wires Clim Change 8:e454. https://doi.org/10.1002/wcc.454

Bay L, Quigley K, Randall C, Negri A, van Oppen M, Webster N, Buerger P, Bostrom-Einarsson L, Rocker M, Harrison D, Cleves P (2019) Reef Restoration and Adaptation Program: Intervention technical summary. A report provided to the Australian Government by the Reef Restoration and Adaptation Program. RRAP.

https://gbrrestoration.org/wp-content/uploads/2020/09/T3-Intervention-Technical-Summary-FINAL3.pdf
Beers RF, Sizer IW (1952) A spectrophotometric method for measuring the breakdown of hydrogen peroxide by catalase. J Biol Chem 195:133–140. https://doi.org/10.1016/S0021-9258(19)50881-X
Bhagooli R, Hidaka M (2004a) Photoinhibition, bleaching susceptibility and mortality in two scleractinian corals, *Platygyra ryukyuensis* and *Stylophora pistillata*, in response to thermal and light stresses. Comp Biochem Phys A 137:547–555. https://doi.org/10.1016/j.cbpb.2003.11.008
Bhagooli R, Hidaka M (2004b) Release of zooxanthellae with intact photosynthetic activity by the coral *Galaxea fascicularis* in response to high temperature stress. Mar Biol 145:329–337. https://doi.org/10.1007/s00227-004-1309-7
Bradford MM (1976) A rapid and sensitive method for the quantitation of microgram quantities of protein utilizing the principle of protein-dye binding. Anal Biochem 72:248–254. https://doi.org/10.1006/abio.1976.9999
Bridge TCL, Cowman PF, Quattrini AM, Bonito VE, Sinniger F, Harii S, Head CEI, Hung JY, Halafihi T, Rongo T, Baird AH (2023) A *tenuis* relationship: traditional taxonomy obscures systematics and biogeography of the '*Acropora tenuis*' (Scleractinia: Acroporidae) species complex. Zool J Linn Soc 202:1–24. https://doi.org/10.1093/zoolinnean/zlad062
Brown A, Pfab F, Baxter E, Detmer A, Moeller H, Nisbet R, Cunning R (2022) Analysis of a mechanistic model of corals in association with multiple symbionts: within-host competition and recovery from bleaching. Conserv Physiol. https://doi.org/10.1093/conphys/coac066
Butcherine P, Tagliafico A, Ellis SL, Kelaher BP, Hendrickson C, Harrison D (2023) Intermittent shading can moderate coral bleaching on shallow reefs. Front Mar Sci. https://doi.org/10.3389/fmars.2023.1162896
Cantin NE, James N, Stella J (2024) Aerial surveys of the 2024 mass coral bleaching event on the Great Barrier Reef. Retrieved May 21, 2024, from https://www.aims.gov.au/research-topics/environmental-issues/coral-bleaching/coral-bleaching-events
Castro-Sanguino C, Stick D, Duffy S, Grimaldi C, Gilmour J, Thomas L (2024) Differential impacts of light on coral phenotypic responses to acute heat stress. J Exp Mar Biol Ecol. https://doi.org/10.1016/j.jembe.2024.152057
Clarke KR, Gorley RN (2006) *PRIMER v6: User Manual/tutorial (Plymouth Routines in Multivariate Ecological Research)*. PRIMER-E Ltd.
Coelho V, Fenner D, Caruso C, Bayles B, Huang Y, Birkeland C (2017) Shading as a mitigation tool for coral bleaching in three common Indo-Pacific species. J Exp Mar Biol Ecol 497:152–163. https://doi.org/10.1016/j.jembe.2017.09.016
Coles SL, Jokiel PL (1978) Synergistic effects of temperature, salinity and light on the hermatypic coral *Montipora verrucosa*. Mar Biol 49:187–195. https://doi.org/10.1007/BF00391130
Comeau S, Carpenter RC, Edmunds PJ (2014) Effects of irradiance on the response of the coral *Acropora pulchra* and the calcifying alga *Hydrolithon reinboldii* to temperature elevation and ocean acidification. J Exp Mar Biol Ecol 453:28–35. https://doi.org/10.1016/j.jembe.2013.12.013
Cunning R, Silverstein RN, Baker AC (2015) Investigating the causes and consequences of symbiont shuffling in a multi-partner reef coral symbiosis under environmental change. Proc Biol Sci. https://doi.org/10.1098/rspb.2014.1725
Cunning R, Muller EB, Gates RD, Nisbet RM (2017) A dynamic bioenergetic model for coral-*Symbiodinium* symbioses and coral bleaching as an alternate stable state. J Theor Biol 431:49–62. https://doi.org/10.1016/j.jtbi.2017.08.003
DeCarlo TM, Cohen AL, Wong GTF, Davis KA, Lohmann P, Soong K (2017) Mass coral mortality under local amplification of 2 °C ocean warming. Sci Rep 7:Article 44586. https://doi.org/10.1038/srep44586
Ellis SL, Butcherine P, Tagliafico A, Hendrickson C, Kelaher BP, Schulz KG, Harrison DP (2024) Shading responses are species-specific in thermally stressed corals. Front Mar Sci. https://doi.org/10.3389/fmars.2024.1333806
Ellis SL, Baird ME, Harrison LP, Schulz KG, Harrison DP (2025b) A photophysiological model of coral bleaching under light and temperature stress: experimental assessment. Conserv Physiol. https://doi.org/10.1093/conphys/coaf020
Ellis SL, Baird ME, Butcherine P, Fiori AT, Harrison LP, Hendrickson C, Schulz KG, Harrison DP (2025a) CBM_experimental_validation. https://doi.org/10.5281/zenodo.17098791
Eynaud Y, Nisbet RM, Muller EB (2011) Impact of excess and harmful radiation on energy budgets in scleractinian corals. Ecol Model 222(7):1315–1322. https://doi.org/10.1016/j.ecolmodel.2011.01.004
Fitt WK, Brown BE, Warner ME, Dunne RP (2001) Coral bleaching: interpretation of thermal tolerance limits and thermal thresholds in tropical corals. Coral Reefs 20:51–65. https://doi.org/10.1007/s003380100146
Goyen S, Pernice M, Szabó M, Warner ME, Ralph PJ, Suggett DJ (2017) A molecular physiology basis for functional diversity of hydrogen peroxide production amongst *Symbiodinium* spp. (Dinophyceae). Mar Biol 164:46. https://doi.org/10.1007/s00227-017-3073-5
Harrison DP, Harrison L, Baird M, Utembe S, Schofield R, Escobar Correa R, Mongin M, Rizwi F (2019) Reef Restoration and Adaptation Program: Environmental modelling of large scale solar radiation management. A report provided to the Australian Government by the Reef Restoration and Adaptation Program. RRAP. https://gbrrestoration.org/resources/reports/
Harrison DP (2024) An overview of environmental engineering methods for reducing coral bleaching stress. In E. Wolanski & M. Kingsford (Eds.), *Oceanographic processes of coral reefs* (2nd ed., pp. 403–418). CRC Press. https://doi.org/10.1201/9781003320425-31
Helgoe J, Davy SK, Weis VM, Rodriguez-Lanetty M (2024) Triggers, cascades, and endpoints: connecting the dots of coral bleaching mechanisms. Biol Rev 99:715–752. https://doi.org/10.1111/brv.13042
Heron SF, Johnston L, Liu G, Geiger EF, Maynard JA, De La Cour JL, Johnson S, Okano R, Benavente D, Burgess TFR, Iguel J, Perez DI, Skirving WJ, Strong AE, Tirak K, Eakin CM (2016) Validation of reef-scale thermal stress satellite products for coral bleaching monitoring. Remote Sens 8(1):59. https://doi.org/10.3390/rs8010059
Higuchi T, Yuyama I, Nakamura T (2015) The combined effects of nitrate with high temperature and high light intensity on coral bleaching and antioxidant enzyme activities. Reg Stud Mar Sci 2:27–31. https://doi.org/10.1016/j.rsma.2015.08.012
Hobday AJ, Alexander LV, Perkins SE, Smale DA, Straub SC, Oliver ECJ, Benthuysen JA, Burrows MT, Donat MG, Feng M, Holbrook NJ, Moore PJ, Scannell HA, Sen Gupta A, Wernberg T (2016) A hierarchical approach to defining marine heatwaves. Prog Oceanogr 141:227–238. https://doi.org/10.1016/j.pocean.2015.12.014
Hoegh-Guldberg O (1999) Climate change, coral bleaching and the future of the world's coral reefs. Mar Freshwater Res 50(8):839–866. https://doi.org/10.1071/MF99078
Hoegh-Guldberg O, Smith GJ (1989) The effect of sudden changes in temperature, light and salinity on the population density and export of zooxanthellae from the reef corals *Stylophora pistillata* Esper and *Seriatopora hystrix* Dana. J Exp Mar Biol Ecol 129(3):279–303. https://doi.org/10.1016/0022-0981(89)90109-3
Hughes TP, Anderson KD, Connolly SR, Heron SF, Kerry JT, Lough JM, Baird AH, Baum JK, Berumen ML, Bridge TC, Claar DC,

Eakin CM, Gilmour JP, Graham NAJ, Harrison H, Hobbs J-PA, Hoey AS, Hoogenboom M, Lowe RJ, McCulloch MT, Pandolfi JM, Pratchett M, Schoepf V, Torda G, Wilson SK (2018) Spatial and temporal patterns of mass bleaching of corals in the Anthropocene. Science 359(6371):80–83. https://doi.org/10.1126/science.aan8048

IPCC (2021) Climate change 2021: The physical science basis. Contribution of working group I to the sixth assessment report of the Intergovernmental Panel on Climate Change. Cambridge University Press, Cambridge

Jeans J, Szabó M, Campbell DA, Larkum AWD, Ralph PJ, Hill R (2014) Thermal bleaching induced changes in photosystem II function not reflected by changes in photosystem II protein content of *Stylophora pistillata*. Coral Reefs 33:131–139. https://doi.org/10.1007/s00338-013-1091-4

Jones RJ (1997) Changes in zooxanthellar densities and chlorophyll concentrations in corals during and after a bleaching event. Mar Ecol Prog Ser 158:51–59. https://doi.org/10.3354/meps158051

Jones RJ, Hoegh-Guldberg O, Larkum AWD, Schreiber U (1998) Temperature-induced bleaching of corals begins with impairment of the CO_2 fixation mechanism in zooxanthellae. Plant Cell Environ 21(12):1219–1230. https://doi.org/10.1046/j.1365-3040.1998.00345.x

Jones RJ, Ward S, Amri AY, Hoegh-Guldberg O (2000) Changes in quantum efficiency of Photosystem II of symbiotic dinoflagellates of corals after heat stress, and of bleached corals sampled after the 1998 Great Barrier Reef mass bleaching event. Mar Freshwater Res 51(1):63–71. https://doi.org/10.1071/MF99100

Kramer J, Ripkey N, Segard L, Troisi M, Kramer P, Coraspe P, Waldera C, Kramer P, Ripkey B (2016) Turn down the heat–an innovative citizen science pilot project to reduce impacts of coral bleaching [Paper presentation]. In: Proceedings of the 69th Gulf and Caribbean Fisheries Institute, Grand Cayman, Cayman Islands

Larsen TC, Browne NK, Erichsen AC, Tun K, Todd PA (2017) Modelling for management: coral photo-physiology and growth potential under varying turbidity regimes. Ecol Model 362:1–12. https://doi.org/10.1016/j.ecolmodel.2017.08.018

Leahy SM, Kingsford MJ, Steinberg CR (2013) Do clouds save the Great Barrier Reef? Satellite imagery elucidates the cloud-SST relationship at the local scale. PLoS ONE 8(7):e70400. https://doi.org/10.1371/journal.pone.0070400

Lesser MP (1997) Oxidative stress causes coral bleaching during exposure to elevated temperatures. Coral Reefs 16:187–192. https://doi.org/10.1007/s003380050073

Lesser MP (2010) Coral bleaching: causes and mechanisms. Springer, Netherlands

Li Y, Schellhorn HE (2007) Rapid kinetic microassay for catalase activity. J Biomol Tech 18(4):185–187

Martell HA, Zimmerman RC (2021) Heating rate modulates the metabolic response of the staghorn coral *Acropora cervicornis* (Lamarck, 1816). Mar Biol 168:83. https://doi.org/10.1007/s00227-021-03847-6

MATLAB (2023) MATLAB (v23.2.0.2409890 Update 3). The MathWorks Inc. https://au.mathworks.com/products/matlab.html

McLachlan RH, Grottoli AG (2021) Image analysis to quantify coral bleaching using greyscale model. Protocolsio. https://doi.org/10.17504/protocols.io.bx8wprxe

Messer LF, Bourne DG, Robbins SJ, Clay M, Bell SC, McIlroy SJ, Tyson GW (2024) A genome-centric view of the role of the *Acropora kenti* microbiome in coral health and resilience. Nat Commun 15(1):2902. https://doi.org/10.1038/s41467-024-46905-5

Middlebrook R, Hoegh-Guldberg O, Leggat W (2008) The effect of thermal history on the susceptibility of reef-building corals to thermal stress. J Exp Biol 211(7):1050–1056. https://doi.org/10.1242/jeb.013284

Middlebrook R, Anthony KRN, Hoegh-Guldberg O, Dove S (2010) Heating rate and symbiont productivity are key factors determining thermal stress in the reef-building coral *Acropora formosa*. J Exp Biol 213(7):1026–1034. https://doi.org/10.1242/jeb.031633

Miller J, Muller E, Rogers C, Waara R, Atkinson A, Whelan KRT, Patterson M, Witcher B (2009) Coral disease following massive bleaching in 2005 causes 60% decline in coral cover on reefs in the US Virgin Islands. Coral Reefs 28:925–937. https://doi.org/10.1007/s00338-009-0531-7

Muller EB, Kooijman SALM, Edmunds PJ, Doyle FJ, Nisbet RM (2009) Dynamic energy budgets in syntrophic symbiotic relationships between heterotrophic hosts and photoautotrophic symbionts. J Theor Biol 259(1):44–57. https://doi.org/10.1016/j.jtbi.2009.03.004

Mumby PJ, Chisholm JRM, Edwards AJ, Clark CD, Roark EB, Andrefouet S, Jaubert J (2001) Unprecedented bleaching-induced mortality in *Porites* spp. at Rangiroa Atoll. French Polynesia Mar Biol 139:183–189. https://doi.org/10.1007/s002270100575

Murphy MP, Bayir H, Belousov V, Chang CJ, Davies KJA, Davies MJ, Dick TP, Finkel T, Forman HJ, Janssen-Heininger Y, Gems D, Kagan VE, Kalyanaraman B, Larsson N-G, Milne GL, Nyström T, Poulsen HE, Radi R, Van Remmen H, Schumacker PT, Thornalley PJ, Toyokuni S, Winterbourn CC, Yin H, Halliwell B (2022) Guidelines for measuring reactive oxygen species and oxidative damage in cells and in vivo. Nat Metab 4:651–662. https://doi.org/10.1038/s42255-022-00591-z

Oliver ECJ, Donat MG, Burrows MT, Moore PJ, Smale DA, Alexander LV, Benthuysen JA, Feng M, Sen Gupta A, Hobday AJ, Holbrook NJ, Perkins-Kirkpatrick SE, Scannell HA, Straub SC, Wernberg T (2018) Longer and more frequent marine heatwaves over the past century. Nat Commun 9:1324. https://doi.org/10.1038/s41467-018-03732-9

Oliver ECJ, Burrows MT, Donat MG, Sen Gupta A, Alexander LV, Perkins-Kirkpatrick SE, Benthuysen JA, Hobday AJ, Holbrook NJ, Moore PJ, Thomsen MS, Wernberg T, Smale DA (2019) Projected marine heatwaves in the 21st century and the potential for ecological impact. Front Mar Sci 6:734. https://doi.org/10.3389/fmars.2019.00734

Piggot AM, Fouke BW, Sivaguru M, Sanford RA, Gaskins HR (2009) Change in zooxanthellae and mucocyte tissue density as an adaptive response to environmental stress by the coral, *Montastraea annularis*. Mar Biol 156:2379–2389. https://doi.org/10.1007/s00227-009-1267-1

Ragni M, Airs RL, Hennige SJ, Suggett DJ, Warner ME, Geider RJ (2010) PSII photoinhibition and photorepair in *Symbiodinium* (Pyrrhophyta) differs between thermally tolerant and sensitive phylotypes. Mar Ecol Prog Ser 406:57–70. https://doi.org/10.3354/meps08571

Rangel MS, Erler D, Tagliafico A, Cowden K, Scheffers S, Christidis L (2019) Quantifying the transfer of prey δ15N signatures into coral holobiont nitrogen pools. Mar Ecol Prog Ser 610:33–49. https://doi.org/10.3354/meps12847

Richards LS, Siems ST, Huang Y, Zhao W, Harrison DP, Manton MJ, Reeder MJ (2024) The meteorological drivers of mass coral bleaching on the central Great Barrier Reef during the 2022 La Niña. Sci Rep 14:Article 23867. https://doi.org/10.1038/s41598-024-74181-2

Sahin D, Schoepf V, Filbee-Dexter K, Thomson DP, Radford B, Wernberg T (2023) Heating rate explains species-specific coral bleaching severity during a simulated marine heatwave. Mar Ecol Prog Ser 706:33–46. https://doi.org/10.3354/meps14246

Scofield JMP, Prime EL, Flores F, Severati A, Mongin M, Bougeot E, Baird ME, Negri AP, Qiao GG (2024) The development of a floating mono-particle "Sun Shield" to protect corals from high irradiance during bleaching conditions. J Mar Sci Eng. https://doi.org/10.3390/jmse12101809

Silverstein RN, Cunning R, Baker AC (2017) Tenacious D: *Symbiodinium* in clade D remain in reef corals at both high and low temperature extremes despite impairment. J Exp Biol 220(7):1192–1196. https://doi.org/10.1242/jeb.148239

Stewart H, Kline D, Chapman L, Altieri A (2021) Caribbean mangrove forests act as coral refugia by reducing light stress and increasing coral richness. Ecosphere 12:e03413. https://doi.org/10.1002/ecs2.3413

Stimson J (1985) The effect of shading by the table coral *Acropora hyacinthus* on understory corals. Ecology 66(1):40–53. https://doi.org/10.2307/1941305

Suggett DJ, Warner ME, Smith DJ, Davey P, Hennige S, Baker NR (2008) Photosynthesis and production of hydrogen peroxide by *Symbiodinium* (Pyrrhophyta) phylotypes with different thermal tolerances. J Phycol 44(4):948–956. https://doi.org/10.1111/j.1529-8817.2008.00537.x

Suggett DJ, Macintyre HL, Kana TM, Geider RJ (2009) Comparing electron transport with gas exchange: parameterising exchange rates between alternative photosynthetic currencies for eukaryotic phytoplankton. Aquat Microb Ecol 56:147–162. https://doi.org/10.3354/ame01303

Sun Y, Oberley LW, Li Y (1988) A simple method for clinical assay of superoxide dismutase. Clin Chem 34(3):497–500. https://doi.org/10.1093/clinchem/34.3.497

Tagliafico A, Baker P, Kelaher B, Ellis S, Harrison D (2022) The effects of shade and light on corals in the context of coral bleaching and shading technologies. Front Mar Sci 9:919382

Tchernov D, Gorbunov MY, de Vargas C, Narayan Yadav S, Milligan AJ, Häggblom M, Falkowski PG (2004) Membrane lipids of symbiotic algae are diagnostic of sensitivity to thermal bleaching in corals. P Natl Acad Sci USA 101(37):13531–13535. https://doi.org/10.1073/pnas.0402907101

Teixeira CD, Leitão RLL, Ribeiro FV, Moraes FC, Neves LM, Bastos AC, Pereira-Filho GH, Kampel M, Salomon PS, Sá JA, Falsarella LN, Amario M, Abieri ML, Pereira RC, Amado-Filho GM, Moura RL (2019) Sustained mass coral bleaching (2016–2017) in Brazilian turbid-zone reefs: taxonomic, cross-shelf and habitat-related trends. Coral Reefs 38:801–813. https://doi.org/10.1007/s00338-019-01789-6

Theilacker G, Kimball A (1984) Comparative quality of rotifers and copepods as food for larval fishes. Cal Coop Ocean Fish 25:80–86

Tyystjärvi E (2013) Chapter Seven - Photoinhibition of photosystem II *. In: Jeon KW (ed) International review of cell and molecular biology. Academic Press, Amsterdam, pp 243–303

Vanhaecke P, Sorgeloos P (1980) International study on *Artemia* IV: The biometrics of Artemia strains from different geographical origin. In The brine shrimp Artemia: Proceedings of the International Symposium on the brine shrimp Artemia salina, Corpus Christi (pp. 393–405). Universa Press: Wetteren

Weydert CJ, Cullen JJ (2010) Measurement of superoxide dismutase, catalase and glutathione peroxidase in cultured cells and tissue. Nat Protoc 5:51–66. https://doi.org/10.1038/nprot.2009.197